Nuclear Instruments and Methods in Physics Research A 1091 (2026) 171764

Contents lists available at ScienceDirect

Nuclear Inst. and Methods in Physics Research, A

journal homepage: www.elsevier.com/locate/nima

Full Length Article

Characterization and applications of the $LaBr_3$ array at HUN-REN ATOMKI

L. Csedreki [a,b,*], M. Begala [a,c], M.M. Juhász [a], D. Sohler [a], Z. Elekes [a,b,d], A.J. Krasznahorkay [a]

[a] HUN-REN Institute for Nuclear Research (HUN-REN ATOMKI), PO Box 51, 4001 Debrecen, Hungary
[b] HUN-REN Office for Supported Research Groups, Alkotmány u. 29., 1054 Budapest, Hungary
[c] University of Debrecen, Doctoral School of Physics, Bem tér 18/c, 4026 Debrecen, Hungary
[d] University of Debrecen, Institute of Physics, Faculty of Science and Technology, Egyetem tér 1, H-4032 Debrecen, Hungary

ARTICLE INFO

Keywords:
$LaBr_3$ scintillators
Nuclear Physics
Nuclear astrophysics
Geant4
PSD

ABSTRACT

A high-efficiency γ-ray spectrometer at HUN-REN Institute for Nuclear Research (HUN-REN ATOMKI), the LAnthanum Bromide Detector Array (LABDA) has been designed and constructed to study low-probability phenomena in particle physics, nuclear spectroscopy, and nuclear astrophysics experiments. The array is comprised of 12 cylindrically shaped $LaBr_3$(Ce) crystals, each measuring $3'' \times 3''$, produced by Saint-Gobain. Key performance parameters of the array have been systematically characterized over a broad γ-ray energy range (344–10762 keV), including energy resolution, energy non-linearity, detection efficiency, time resolution and intrinsic background. Intrinsic background suppression, using pulse-shape discrimination methods has been also investigated. The prospects for applying the array to different nuclear physics measurements are discussed.

1. Introduction

Over the past two decades, $LaBr_3$(Ce) detectors have emerged as a highly promising alternative to traditional inorganic scintillators such as NaI(Tl) and BaF_2 in γ-ray spectroscopy. Their superior properties – fast scintillation decay time ($\sim$ 16 ns), high crystal density ($\sim$ 5.08 g/cm^3), substantial light output (63 photons/keV), excellent temperature stability, good linearity for γ rays below 10 MeV, and significantly improved energy resolution ($\sim$ 3% at 662 keV [1]) – make them suitable for a broad range of particle, nuclear, and astrophysical applications [2–5]. The materials high effective atomic number (Z_{La} = 57, Z_{Br} = 35) results in larger photon absorption compared with germanium-based detectors at similar density, and its peak emission wavelength ($\sim$ 380 nm) is well matched to the commonly used photocathodes of photomultipliers (PMT). Combined with its excellent timing performance and resistance to radiation damage, these properties support its use in high-rate experiments and radioactive ion beam studies, including measurements in neutron-rich environments [6,7].

Despite these advantages, $LaBr_3$(Ce) detectors exhibit a significant intrinsic background due to the decay of ^{138}La and ^{227}Ac impurities [4,8,9]. This background constrains their applicability in medium γ-ray measurements (below 2800 keV), particularly in studies of low cross-section nuclear reactions. However, pulse-shape discrimination (PSD) methods and waveform-analysis algorithms can be employed to improve the timing resolution and background suppression [10–12].

Overall, these properties make $LaBr_3$(Ce) detectors attractive for modern nuclear spectroscopy, like the measurement of the high-energy decay of the ^{7}Li(p, γ)^{8}Be reaction important for light boson research; nuclear astrophysics including investigation of radiative nuclear reactions, such as ^{12,13}C(p, γ)^{13,14}N, ^{14}N(p, γ)^{15}O and ^{17}O(p, γ)^{18}F; as well as nuclear applications, *e.g.* study of the ^{51}V(p,n)^{51}Cr reaction.

Utilizing these capabilities the LAnthanum Bromide Detector Array (LABDA) at HUN-REN ATOMKI was originally constructed to measure $\gamma - \gamma$ coincidences associated with the ~10 MeV double γ-decay of the hypothetical X(17) particle [13]. These experiments require a detection system with high efficiency at high-energy γ-ray energies and low background for the identification of very rare events. For this purpose, an array consisting of relatively large $3''\times3''$ $LaBr_3$(Ce) crystals proved to be particularly suitable. In addition to the continuation of experiments dedicated to this subject [14], the array was also used for studies of reactions relevant to nuclear astrophysics (^{14}N(p, γ)^{15}O) and nuclear applications research (^{51}V(p,n)^{51}Cr).

This work provides a systematic study of the LABDA-array performance, with particular emphasis on the characterization of the large-volume $LaBr_3$(Ce) detectors at high γ-ray energies, intrinsic background suppression using PSD techniques, and benchmarking against existing $LaBr_3$(Ce)-based arrays. The experimental arrangement of the LABDA array used for nuclear physics experiments, together with the conditions under which the performance tests of individual detectors

* Corresponding author.
E-mail address: csedreki@atomki.hu (L. Csedreki).

https://doi.org/10.1016/j.nima.2026.171764
Received 31 March 2026; Received in revised form 10 June 2026; Accepted 10 June 2026
Available online 19 June 2026

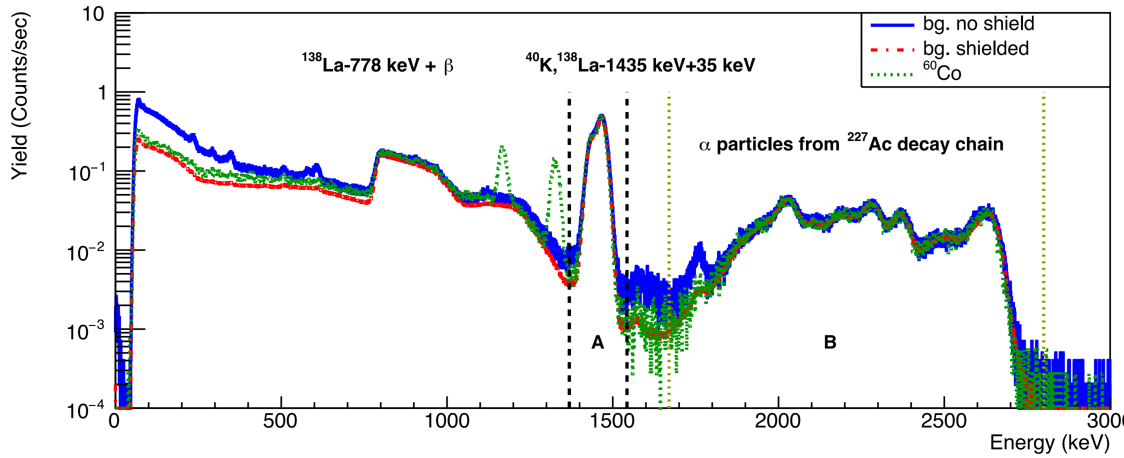

Fig. 1. Experimental spectra of a single $LaBr_3$(Ce) detector. Background condition in a shielded (dashed line) and a non-shielded (solid line) configuration is shown together with a ^{60}Co source (dotted line). Vertical lines indicate the different integrated energy regions (**A**: dashed lines E_1 = 1370–1540 keV, **B**: dotted lines E_2 = 1660–2760 keV)), used to evaluate the background suppression in different configurations.

were carried out, is presented in Section 2. The intrinsic background characteristics of the scintillators in different configurations are discussed in Section 3, along with key performance metrics of the detector array, including energy resolution, linearity, long-term stability, time resolution and photopeak efficiency. Geant4 simulations of the response of the array and comparisons with experimental data are reported in Section 4. Various PSD approaches used to suppress the intrinsic scintillator background are introduced in Section 5. Finally, Section 6 presents the commissioning measurements demonstrating the application of $LaBr_3$(Ce) scintillators at HUN-REN ATOMKI.

2. Experimental methods

The LABDA scintillator array consists of 12 $LaBr_3$(Ce) detectors based on $3'' \times 3''$ Saint-Gobain crystals each coupled to a Hamamatsu R10233 PMT. The PMT's are equipped with Hamamatsu E1198-26 resistive voltage dividers supplemented by active semiconductor components to stabilize the voltages of the final dynodes under high-counting rate conditions.

Depending on the choice of PMT, voltage divider and applied voltage, significant deviations from the ideal linear energy-to-charge response, as well as pulse shape distortions can occur, especially for high-energy γ-rays. To mitigate these effects, Giaz et al. [15] developed a dedicated voltage divider incorporating active components, specifically optimized for large-volume $LaBr_3$(Ce) scintillation detectors, which significantly reduce such nonlinearities. The implementation of similar divider designs is planned for future upgrades of the array.

The detectors are mounted on a hemispherical support structure that provides large solid-angle coverage and allows adjustment of the target–detector distance within the 100–200 mm range.

In the standard configuration, 12 $LaBr_3$(Ce) detectors are arranged on two concentric rings at polar angles of 41.97° (4 detectors) and 78.69° (8 detectors) with respect to the beam direction. The default target-detector distance is 200 mm. A series of test measurements were conducted to characterize the $LaBr_3$(Ce) detectors, focusing on the intrinsic background, energy resolution, energy linearity, photopeak detection efficiency, and the applicability of PSD methods for intrinsic background suppression.

As a first step, the intrinsic background of the individual detectors was investigated at a low background station consisting of a multilayer shielding of 50 mm of lead and 100 mm of paraffin. In addition, standard radioactive sources such as ^{60}Co, ^{137}Cs, ^{152}Eu were also used to provide reference data for the Geant4 simulation of the scintillator response (see Section 4 for details).

The source measurements were complemented with an investigation of the ^{27}Al(p, γ)^{28}Si radiative capture reaction at E_p = 992 keV with a Q value of 11584.9 keV in order to extend the γ-ray energy range up to 10762 keV (for more details see Table 1. in Ref. [16]). The measurements were performed at the 2.0 MV Medium-Current Plus Tandetron Accelerator of HUN-REN ATOMKI [17].

For the study of the ^{27}Al(p, γ)^{28}Si reaction, ^{27}Al was evaporated onto a 0.25 mm thick tantalum backing. The resulting aluminium layer corresponded to a proton energy loss of approx. 15 keV at E_p = 992 keV. The targets were irradiated at the nuclear astrophysics vacuum chamber (for more details see [18]), which is equipped with a 250 mm long extension tube that enables the placement of multiple detectors around the target position.

The beam size on the target was 5 mm in diameter, defined by a tantalum aperture at the entrance of the chamber. The entire chamber functioned as a Faraday cup for beam charge integration. The charge was measured by an ORTEC 439 Digital Current Integrator. Beam currents ranged from 0.5 μA and 4 μA, depending on the reaction cross section. The targets acted as the beam stop and closure of the vacuum chamber and were actively cooled by airflow to maintain thermal stability.

A CAEN Sy5527LS high voltage power supply was used to bias the PMT's of the detectors with voltages between −600 V and −750 V. Detector signals were digitized using a CAEN DT5725 8 channel 14-bit 250 MS/s desktop digitizer with pulse height analysis firmware implementing a trapezoidal shaping algorithm (CAEN DPP-PHA) [19]. The digitizer served as the default data acquisition system (DAQ), using trapezoidal shaping parameters of 288 ns rise time and a flat top of 144 ns. All anode signals, without preamplification, were processed directly by the digitizer. Data were acquired in list mode, storing the calculated energy and timestamp of each event. The dead time remained below 2% throughout the measurements. To suppress the alpha induced intrinsic background in the 1700–2800 keV energy range, different PSD techniques were investigated. During these PSD studies and to determine the time resolution of the individual detectors, signals were recorded using a CAEN V1730D 14-bit 500 MS/s digitizer.

3. Results and discussion

3.1. Detector background

$LaBr_3$(Ce) scintillators exhibit significant intrinsic background primarily from the radioactive decays of ^{138}La, which dominates the γ-ray spectrum below E_γ = 1500 keV. Additionally, alpha particles from the decay of trace actinide impurities present in the material produce a characteristic structure between 1700–2800 keV [9,20] (referred to as the alpha region). Background spectra of a single $LaBr_3$(Ce) detector under different experimental conditions are shown in Fig. 1. The dashed and solid lines represent the background spectra of the detector with and without 50 mm lead shielding, respectively. Intrinsic background lines of ^{138}La and alphas from the decay of daughter nuclei of ^{227}Ac are highlighted. Significant reduction of the ambient background due to the shielding is clearly visible, especially at energies $E_\gamma \leq$500 keV. The vertical lines represent the boundaries of integrated regions (**A** and **B**) for background studies.

The background yields of the 12 detectors in the hemispherical configuration are presented for both shielded and unshielded setups in Fig. 2. The top panel shows the yields, expressed in counts per hour, in the region around the 1470 keV peak (**A**), which includes contributions from the decay of ^{40}K (1460 keV) and ^{138}La (1435 keV plus 31–38 keV as the characteristic X-rays of ^{138}Ba).

The bottom panel displays the integrated yields of the alpha region (**B**). The boundaries of the two regions are indicated by the dashed and dotted energy lines, respectively, in Fig. 1.

A significant difference is observed between the shielded and non-shielded configurations near E_γ ~1470 keV, which is attributed to the presence of environmental ^{40}K. This contributes approximately 15% to the detector background. Among detectors, counting rates are generally consistent within 0.5%, except for one scintillator that shows a ~2% lower rate in the 1470 keV region. An otherwise interesting effect is the level of contaminants of the daughter nuclei of ^{227}Ac decay chain in the alpha region. The discrepancy between the two configurations is ascribed to the shielding of environmental background, which significantly decreases the contribution of the gamma rays in ^{228}Th and ^{226}Ra decay chain, resulting in a reduction at the level of 10%. In addition, the individual detectors show varying counting rates even in the shielded configuration, reflecting differing levels of intrinsic ^{227}Ac contamination present in the detectors, which depend mainly on the production of the scintillators.

3.2. Energy calibration, energy resolution, and detection efficiency measurements

The performance parameters of the LABDA array were determined over a γ-ray energy range of E_γ = 344–10762 keV using standard radioactive sources, laboratory background peaks, and the direct radiative capture reaction on ^{27}Al. Previous studies have reported deviations from linear relationship between the deposited energy and ADC channel at $E_\gamma \leq$0.1 MeV [20] and 9 MeV$\leq E_\gamma$, depending on the voltage applied to the PMT [4,15].

The correlation between the ADC channel number and the deposited energy in a single $LaBr_3$(Ce) scintillator is shown in Fig. 3. Owing to the relatively high voltage (~−700 V), the energy-channel relationship becomes non-linear above 4000 keV, reaching a deviation of about 9%, at 10762 keV. This behavior is consistent with previous results [5]. We concluded that a second-order polynomial was suitable for the energy calibration, producing a deviation of about 0.02%.

The full width at half maximum (FWHM) of the array as a function of γ-ray energy is shown in Fig. 4. The blue symbols and their associated uncertainties represent the mean FWHM value and the standard deviation derived from the 12 detectors at a given energy. The blue curve corresponds to a power-law fit of the form FWHM (%) = 54.86 x $E^{-0.4308}$, where E is expressed in keV. Literature values reported in Ref. [4] for 2″×2″ scintillator crystals are indicated by an orange short-dashed line. In addition, Ref. [9] for 3″×3″ scintillator crystal obtained an energy resolution of 2.1% (FWHM) at 1.33 MeV, which is consistent with our data.

The FWHM of a single detector as a function of the power supply (PS) was also studied over the range PS = −690 and −860 V. The measured values at E_γ = 662, 1173, and 1332 keV as a function of PS values, shown as circles, triangles, and squares, respectively, are presented in Fig. 5. While the energy resolution improves with increasing PS value, by approximately 10% in relative terms, the linearity generally degrades. Indeed, using the A17276 detector, the calculated energy at E_γ = 10.7 MeV deviated by −6.8% and −9.2% at PS values of −600 V and −650 V, respectively.

The total photopeak efficiency (η_{eff}) of the LABDA array was determined using standard radioactive sources and the ^{27}Al(p, γ)^{28}Si radiative capture reaction at the E_p = 992 keV resonance. The reaction yields of the ^{27}Al(p, γ)^{28}Si reaction were corrected for the angular distribution of the emitted γ rays [21] and for the branching ratios of different transitions. Furthermore, a solid-angle correction accounting for the extended detector geometry was applied based on Ref. [22].[1]

The absolute efficiency was determined across the experimental energy range of 500–11000 keV using a simultaneous global least-squares regression. This approach integrates the absolute efficiency measurements from the calibrated radioactive sources (ϵ_{abs}) and the corrected relative γ-ray yields (Y_{rel}) from the reaction.

To model the detector response, we utilized a second-order polynomial expansion in log–log space:

$$\ln(\eta_{eff}) = a + b\ln(E_\gamma) + c(\ln(E_\gamma))^2 \quad (1)$$

where E_γ is the photon energy in keV, and $\{a, b, c\}$ are the free parameters representing the normalization and curvature of the efficiency response.

A critical challenge in high-energy calibration is the lack of absolute activity standards. To resolve this, we introduced a normalization parameter, N, for the reaction data. The global fit minimizes a joint χ^2 function:

$$\chi^2 = \sum_i \left[\frac{\eta_{eff}(E_i) - \epsilon_{abs,i}}{\sigma_{abs,i}}\right]^2 + \sum_j \left[\frac{\eta_{eff}(E_j) - Y_{rel,j}/N}{\sigma_{Y,j}/N}\right]^2 \quad (2)$$

The notations in the function are defined as follows:

- $\epsilon_{abs,i}$ and $\sigma_{abs,i}$ represent the measured absolute efficiency and its associated uncertainty for the ith calibration source transition at energy E_i;
- $Y_{rel,j}$ and $\sigma_{Y,j}$ denote the experimental relative yield and its uncertainty for the jth transition from the nuclear reaction at energy E_j;
- N is the free scaling parameter that maps the relative yield data onto the absolute efficiency scale.

By treating N as a free parameter alongside the shape coefficients, the relative data points are not anchored to a single extrapolated low-energy point. Instead, the entire high-energy dataset is statistically scaled to satisfy the global constraints provided by the absolute standards. This approach utilizes the full shape information of the reaction yields to constrain the efficiency curvature and ensure statistical consistency.

Uncertainties in the efficiency calibration were determined through rigorous error propagation using the full covariance matrix $\mathbf{V}$ obtained from the fit. This matrix accounts for the algebraic correlations between the low-energy normalization and the high-energy slope. The variance of the efficiency σ_η^2 at any given energy E_γ is calculated as:

$$\sigma_\eta^2 = \mathbf{J}^T\mathbf{V}\mathbf{J} \quad (3)$$

where $\mathbf{J}$ is the Jacobian vector containing the partial derivatives of the efficiency function with respect to the parameters $\{\frac{\partial\eta}{\partial a}, \frac{\partial\eta}{\partial b}, \frac{\partial\eta}{\partial c}\}$. This method ensures that systematic uncertainties associated with the scaling of the reaction data and the model extrapolation are naturally incorporated into the final 1σ confidence interval.

[1] The total mass attenuation coefficient was calculated as the weighted sum of the mass attenuation coefficients of the constituents of the compound.

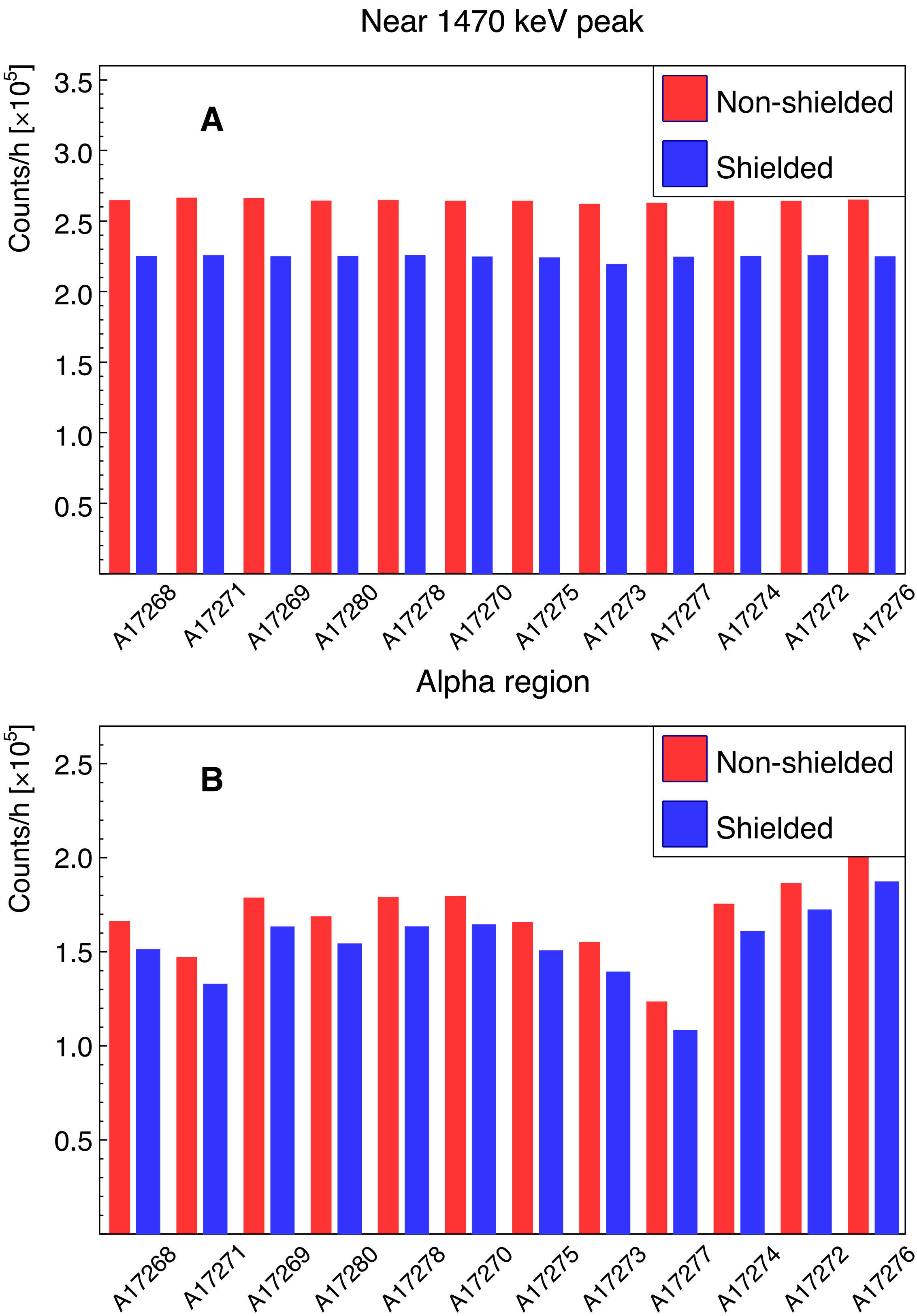

Fig. 2. (Color online) Yields of individual scintillators near the 1470 keV peak (**A**) and in the alpha region (**B**).

To present the performance of the LABDA array, the absolute photopeak efficiencies of the individual detectors were summed for the inner and outer rings and the data were fitted with a second-order polynomial. These data and the resulting fit parameters are presented in Fig. 6. We note here that a significant source of uncertainty is still assigned to the normalization of nuclear reaction data (~10%)

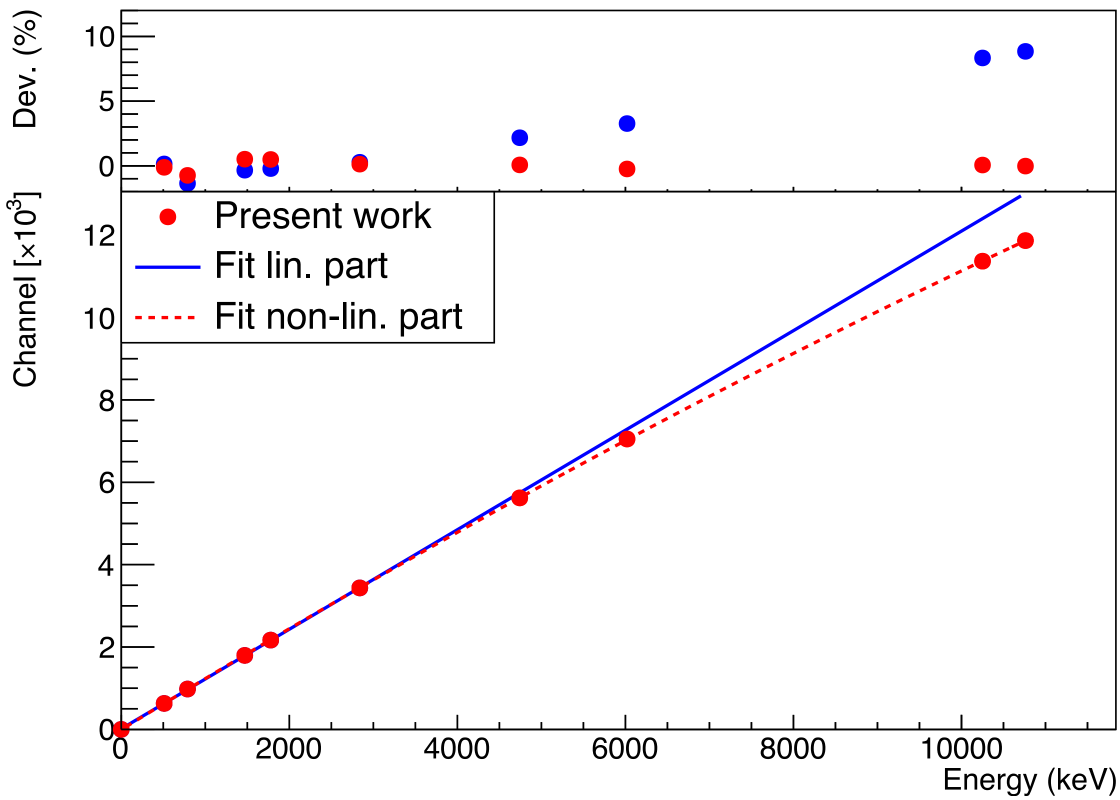

Fig. 3. γ-ray energy as a function of ADC channel number. Solid and dashed lines represent fits to the data in the energy ranges $E_\gamma \leq 4000$ keV and E_γ = 344–10762 keV, respectively. The deviation in percentage terms between the calculated and literature energy values is shown at the top of the figure.

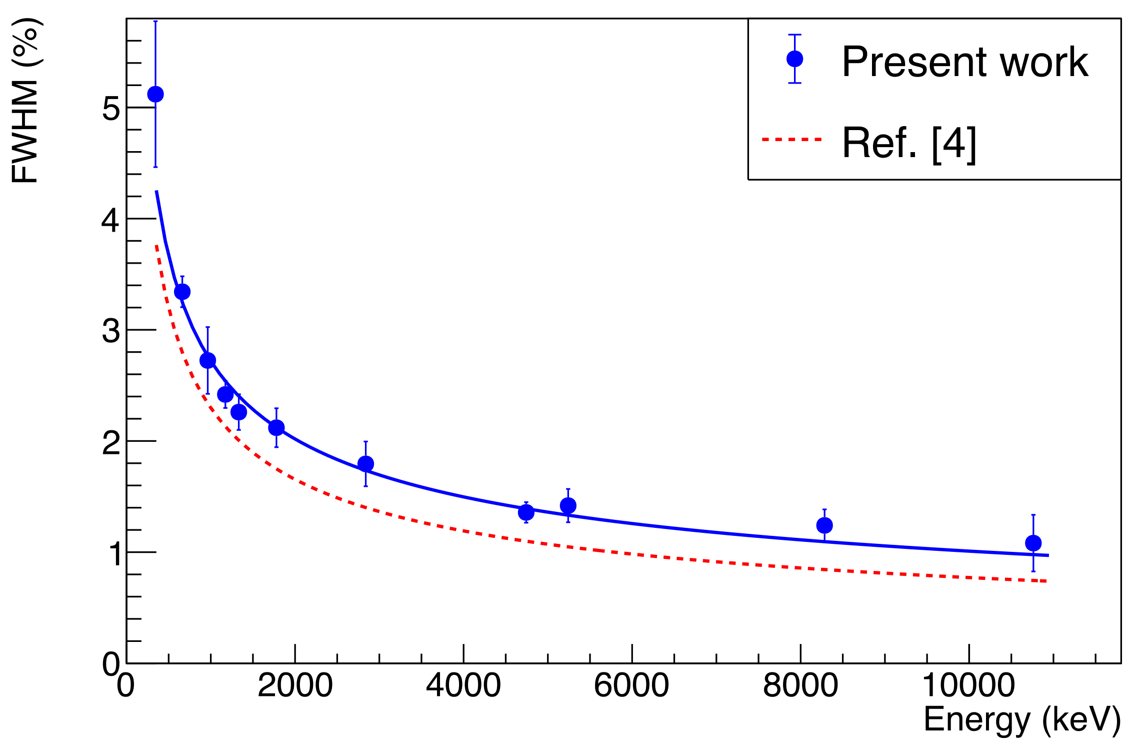

Fig. 4. FWHM as a function of γ-ray energy. Blue symbols and their uncertainties represent the mean FWHM value and the standard deviation derived from the 12 detectors. The blue solid line shows a power-law fit to the data. Literature values from Ref. [4] are indicated by an orange short-dashed line.

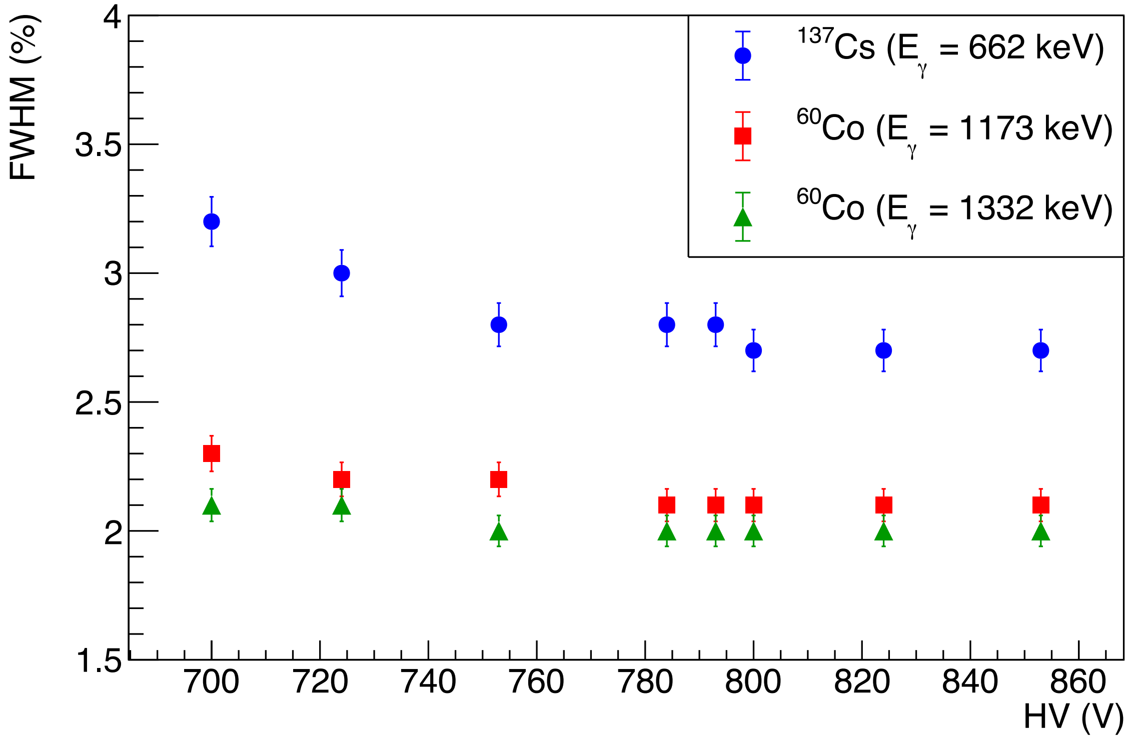

Fig. 5. FWHM of a single detector as a function of power supply voltage.

attributed mainly to the background subtraction of experimental data. This can be improved by the use of radioactive sources with higher energy gammas such as ^{88}Y (with E_γ = 898 and 1836 keV) and/or the ^{14}N(p, γ)^{15}O at E_p = 278 keV (with E_γ = 763, 1380, 2373 and 7554 keV). This will be elaborated and applied in the near future.

3.3. Stability test

Gain instability is a general problem of scintillator detectors [3]. The gain shift arises from different environmental factors that relate both to the detector crystal and to the photomultiplier tube. A well-known source of instability is the fluctuation of the rate of secondary electron emission from the PMT dynodes [23], as well as variations in the scintillation light output of the crystal with changing ambient temperature [24]. Additionally, high counting rates induce voltage fluctuations on the PMT dynodes, further contributing to gain instability.

To study these effects for the LABDA array, a background measurement was performed at the low-background astrophysical laboratory (Site A), where temperature stability can be maintained within $\leq$ 2 C°. Another test was conducted at the Tandetron Laboratory (Site B), where the temperature fluctuations of the accelerator hall and the experimental setup can significantly affect the properties of the detector array. Variation of the peak positions was observed to be below 0.5% and 1% over 14 h of data taking on Sites A and B, respectively. This behavior was consistent across all detectors, indicating a common effect, and it is in agreement with the findings reported in Ref. [3]. Furthermore, the detector parameters were studied as a function of counting rates between 0.3–21 kHz generated with varying source-detector distance using a ^{60}Co radioactive source. We concluded that the parameters remained stable for counting rates of up to 11 kHz with a single detector. This rate is much higher than the general count rates generated in the relevant nuclear reactions in the fields of nuclear astrophysics and particle physics.

3.4. Timing properties

The fast timing performance of the detectors is essential for reducing background in $\gamma\gamma$-coincidence measurements. To characterize the timing performance of the individual detectors in our system, a dedicated measurement was performed using the intense 17.62 MeV γ-radiation produced in the ^{7}Li(p, γ)^{8}Be reaction with a Q value of 17254.4 keV. A thin target (30 μg/cm^2) evaporated onto a 0.5 mm thick Ta backing was irradiated at a proton beam energy of E_p = 450 keV with a beam intensity varying between 4 and 5 μA. The counting rate of the detectors was kept below 1 kHz. The input charge of the detector signals were digitized using a 32-channel CAEN VME V792 QDC (with a ≥4 MeV energy threshold), and the timing was determined using a V812B CFD and digitized using a V775 TDC unit.

The intrinsic timing resolution of the individual detectors was determined through the pairwise coincidence spectra measuring the 17.62 keV gamma photons from the ^{7}Li(p, γ)^{8}Be reaction, with an energy cut set between 8 and 10 MeV to account for partial photon absorption in the detectors. By measuring the FWHM resolution of the coincidence time difference between detector pairs (1–2), (1–3), and (2–3) – denoted by δ_{12}, δ_{13}, and δ_{23}, respectively – the intrinsic FWHM resolutions of the individual detectors (δ_1, δ_2, and δ_3) were extracted.

Assuming the timing uncertainties of the individual detectors are independent and follow a Gaussian distribution, the measured coincidence resolution δ_{ij} relates to the intrinsic resolutions via the quadrature sum $\delta_{ij} = \sqrt{\delta_i^2 + \delta_j^2}$. Consequently, the intrinsic resolution for each detector can be calculated according to:

$$\delta_1 = \sqrt{\frac{\delta_{12}^2 + \delta_{13}^2 - \delta_{23}^2}{2}}, \quad \delta_2 = \sqrt{\frac{\delta_{12}^2 + \delta_{23}^2 - \delta_{13}^2}{2}}, \quad \delta_3 = \sqrt{\frac{\delta_{13}^2 + \delta_{23}^2 - \delta_{12}^2}{2}}.$$

This triplet-based measurement procedure was applied across the array to decouple the timing response of each individual detector. This

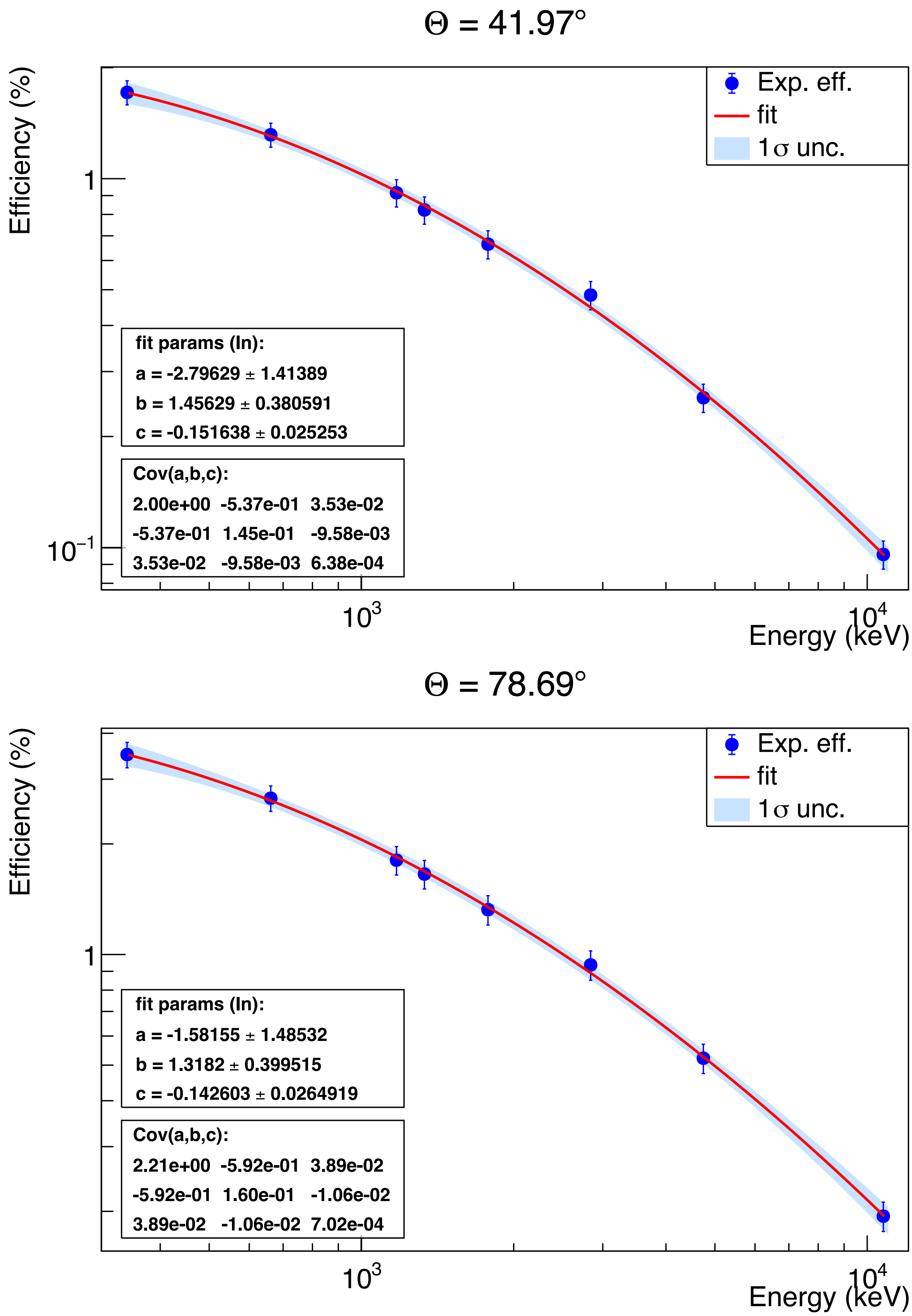

Fig. 6. Total photopeak efficiencies of the LABDA array for the inner (top) and the outer rings (bottom) consisting of 4 and 8 detectors, respectively. Experimental data and the fitted values are represented by blue dots and solid lines, respectively.

approach provides a precise estimate of the intrinsic timing performance for each detector unit without requiring a reference detector of known resolution.

The individual detector parameters, such as detector serial number, energy resolution (defined as FWHM) and timing resolution with the applied PS are presented in Table 1.

Table 1
Detector parameters of the LABDA array.

Detector serial Number	E_{res} as FWHM (%) E_γ = 662 keV	E_γ = 1332 keV	PS (V)	T_{res} as FWHM (ps)	PS (V)
A17268	3.3	2.4	−716	183 ± 14	−589
A17269	3.5	2.3	−700	317 ± 11	−570
A17270	3.2	2.2	−751	352 ± 10	−609
A17271	3.3	2.5	−650	135 ± 21	−540
A17272	3.5	2.3	−640	128 ± 21	−619
A17273	3.2	2.6	−660	199 ± 16	−619
A17274	3.5	2.3	−650	219 ± 14	−584
A17275	3.2	2.0	−660	262 ± 11	−580
A17276	3.3	2.1	−650	238 ± 12	−659
A17277	3.3	2.3	−770	318 ± 11	−580
A17278	3.5	2.3	−700	249 ± 13	−564
A17280	3.1	2.2	−652	298 ± 12–575	
Average	3.3	2.3		242	
St. Dev.	0.1	0.2		72	
Ref. [1]	2.9	2.1		490	

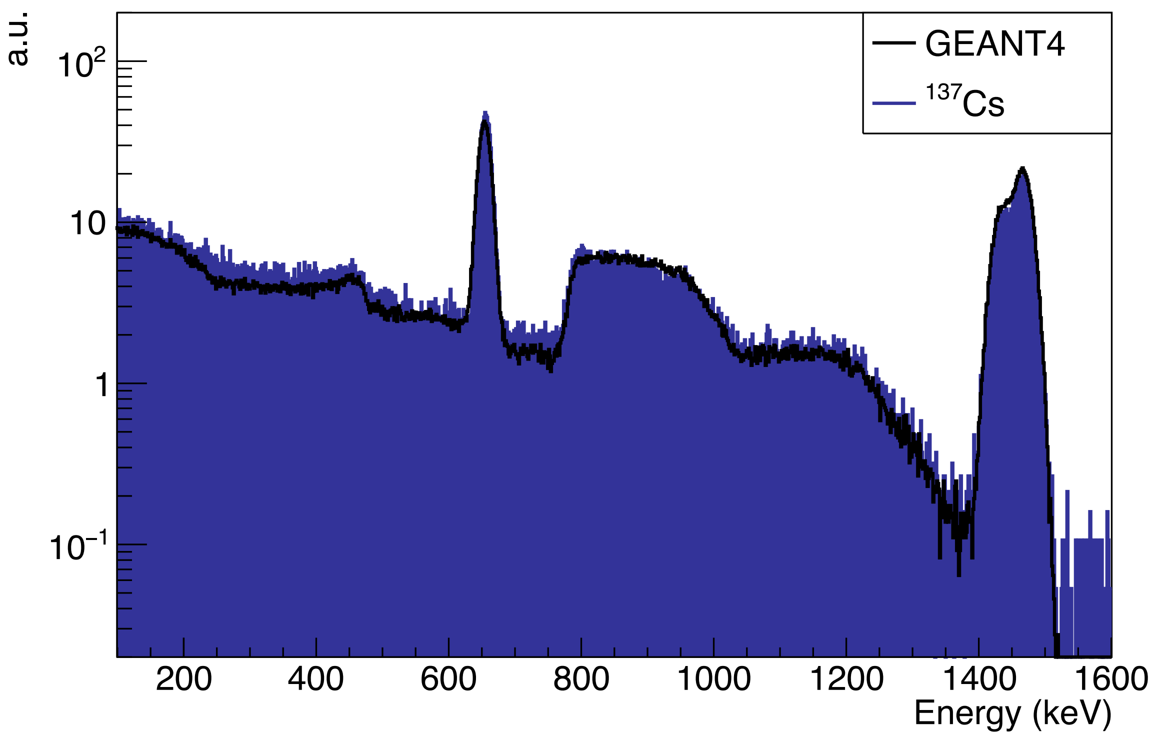

Fig. 7. Simulated and the experimental spectra acquired in a shielded configuration using ^{137}Cs radioactive source.

4. Simulation

The LABDA array was simulated using the Geant4 toolkit [25]. Each detector was modeled as a 3″ × 3″ $LaBr_3$(Ce) crystal covered by a MgO reflector [26], with a front thickness of 2.5 mm and a side thickness of 2.9 mm, based on the mechanical drawing provided by Saint-Gobain. This was enclosed in an aluminium case with a front thickness of 0.8 mm. The PMT was replaced in the model by a 10 mm thick aluminium plate at the rear of the crystal. The standard Geant4 electromagnetic physics list was used, together with G4DecayPhysics("decays") and G4RadioactiveDecayPhysics constructors [27]. Detector resolution was incorporated by applying a Gaussian smearing to the deposited energy, with a standard deviation given by $\sigma = 0.34\times\sqrt{E}$, where E is expressed in keV.

Simulated and experimental spectra acquired in a shielded configuration, using a ^{137}Cs radioactive source at a source-detector distance of 102 mm, are shown in Fig. 7.

The simulated spectrum agrees well with the experimental data. The internal activity of ^{138}La of the crystal was set according to the literature value reported in Ref. [9], while other contaminants from the decay of ^{227}Ac were neglected, since their intensities are one order of magnitude smaller than that of the ^{138}La. Attempts to include them in the simulation yielded no significant difference in the spectrum.

As a next step, the decay of the excited state of ^{28}Si from the ^{27}Al(p, γ)^{28}Si was simulated to obtain η_{eff} in 1500 keV≤E_γ region. We note here that, despite the availability of high-energy simulations of the $LaBr_3$(Ce) scintillator [4,28,29], the comparison of the higher-energy photopeak efficiency data obtained experimentally is limited.

The comparison of the experimental (dotted line) and simulated (dashed and solid lines) spectra in the E_γ= 9000–11 500 keV region[2]

[2] The boundaries of this region were selected due to the absence of γ-ray peaks from nuclear reactions on contaminants. Furthermore, we noted here that the contribution of cosmic-ray background in this region is less than 0.5%.

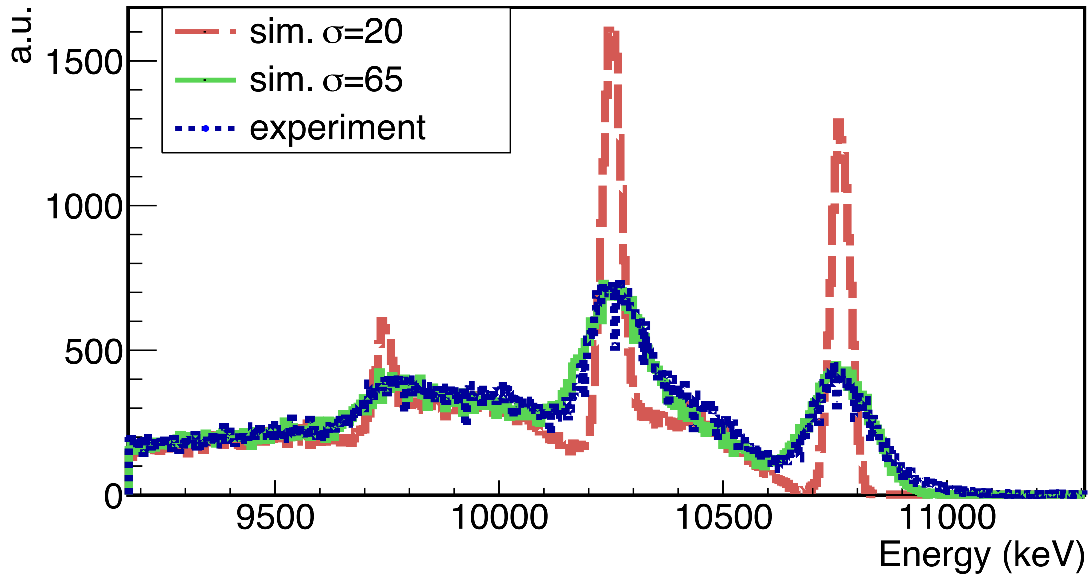

Fig. 8. Comparison of experimental (dotted line) and simulated (straight lines) spectra of ^{27}Al(p, γ)^{28}Si reaction. The simulated spectrum with different energy resolutions are shown with dashed and straight lines, respectively.

is shown in Fig. 8 using different sigma values to represent different energy resolutions. The peak shapes and Compton continuum were used to tune the simulation parameters during the validation. The simulated spectra with different energy resolutions are shown with dashed (σ = 20) and straight (σ = 65) lines, respectively. The results demonstrate that a conventional linear background subtraction in the photopeak region can substantially underestimate the true reaction yield.

The η_{eff} from the simulation was determined using two approaches: first, incorporating the realistic energy resolution and applying the same background subtraction procedure as used for the experimental spectrum (*Sim-biased*); and second, assuming ideal energy resolution without any smearing (*Sim-nonbiased*), corresponding to the true total photopeak efficiency.

Fig. 9 shows the experimental (*Exp*) and simulated photopeak efficiencies (*Sim-biased* and *Sim-nonbiased*) for eight detectors in the outer ring (θ = 78.69°) at a target–detector distance of 200 mm, obtained using linear background subtraction. The impact of the background subtraction on the simulated efficiency is clearly visible. While the values of *Exp* and *Sim-biased* agree within 1 sigma uncertainty, the discrepancy between the *Exp* and *Sim-nonbiased* efficiencies becomes significant for E $_{\gamma}$ ≥ 3000 keV, reaching approximately 35% at E_{γ} = 10762 keV. This deviation beside the Compton-effect, may also be partly due to incomplete modeling of the experimental spectrum, such the Doppler-broadening of experimental peaks or the γ rays from nuclear reactions on impurities (e.g., ^{19}F(p, $\alpha\gamma$)^{16}O). Consequently, the photopeak efficiency curve derived from the experimental data was used to extract nuclear reaction parameters in Section 6.

5. Pulse shape discrimination

To suppress the intrinsic detector background arising from α decays, we investigated the applicability of different PSD methods. For this purpose, data were collected using single-crystal setups in a low-background environment (Site A), with lead and paraffin shielding, and utilizing a CAEN V1730D digitizer.

The differing detection mechanisms of α particles and γ rays result in subtle variations in the shapes of the electrical pulses produced in the detector medium. To quantify these differences, two PSD methods were evaluated to assess their effectiveness in reducing the α-induced background.

The Charge Comparison Method (CCM) was employed because of its straightforward implementation and relatively low dependence on the digitizer sampling rate. In this method, the pulse shape is characterized by integrating the signal over two time intervals. The CCM value is defined as the ratio of the charge integrated over the region of maximal shape difference to the total pulse charge, using a short integration gate of 64 ns and a long integration gate of 144 ns.

The CCM parameters were plotted for energy regions dominated by a single interaction type, namely 1430–1480 keV for γ events and 2200–2500 keV for α events. Each case produced approximately Gaussian distributions, which were then used to define a discrimination threshold, as illustrated in Fig. 10. The threshold was chosen to minimize α-induced counts while preserving the maximum number of γ events.

In addition to the CCM, the data were also analyzed by fitting a simple exponential to the falling edge of each pulse (Falling Edge Fitting Method, FEFM). From the extracted decay constants, we obtained a distribution that clearly separates into two groups, analogous to the CCM results. The discrimination threshold was determined following the same procedure as before.

Both the CCM and the FEFM exhibit reasonable effectiveness in suppressing the intrinsic α-background, which was the primary objective of the analysis. Using the CCM, the α contribution was reduced by 85.2%, while only 10.7% of γ events were inadvertently rejected. The FEFM results in a marginally lower efficiency, achieving a 66.3% reduction in α background and a 16.9% loss of γ events.

It is also worth noting that, although previous works suggest that the PSD efficiency decreases with crystal size (see Refs. [11,30]), the PSD methods applied in the present work still provided good discrimination between the α and γ events, despite the relatively large $3'' \times 3''$ crystal size of the LABDA array.

6. Commissioning

The parameters of the LABDA array compared to some existing $LaBr_3$(Ce) based arrays using for nuclear physics experiments are summarized in Table 2. Our array shows similar performance in terms of FWHM, validated maximum γ energy and η_{eff}. The measured timing

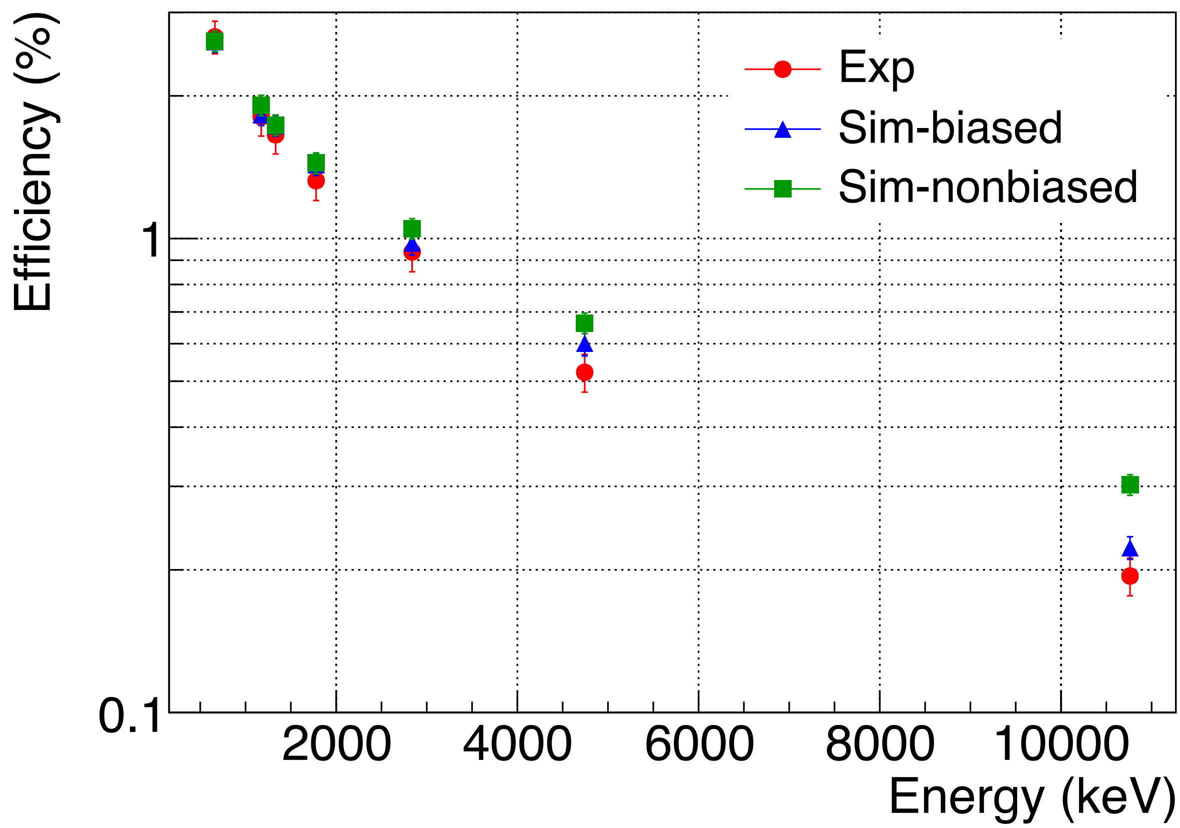

Fig. 9. Experimental (Exp) and the simulated photopeak efficiencies (Sim-biased and Sim-nonbiased) for 8 detectors in the outer ring (θ = 78.69°) at target-detector distance of 200 mm.

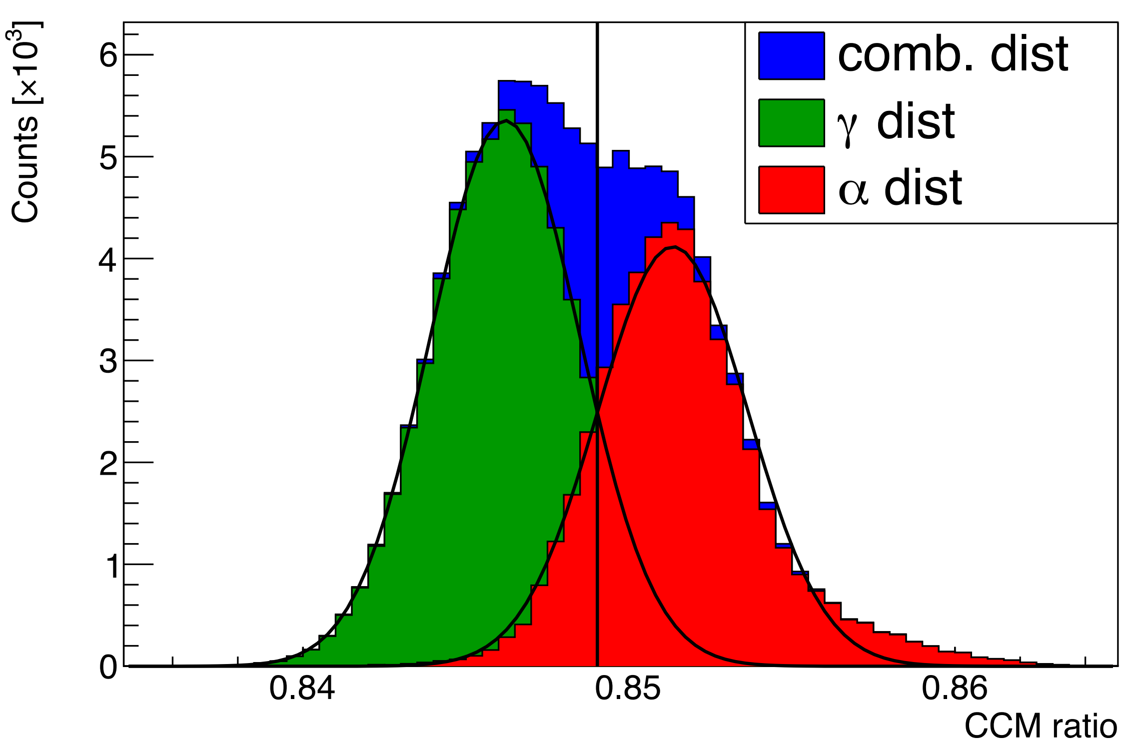

Fig. 10. Distributions of CCM ratios. The γ, the α and the combined distributions are shown in green, red and blue, respectively; the threshold of the discrimination is illustrated with a vertical straight line.

Table 2
Summary of some $LaBr_3$(Ce) arrays used in nuclear physics experiments.

Parameters	Number (pc) and size of detectors	Geometry and solid angle coverage	Energy resolution (FWHM)	Verified Max. E_γ	η_{eff}	Timing resolution
LABDA at ATOMKI	15 pc 3″ × 3″	2 π	2.3(2)% at E_γ = 1332 keV	12 MeV	2.4% at E_γ = 1332 keV	242(72) ps
FATIMA for DESPEC at FAIR [34], [35]	36 pc 1.5″ × 2″	4 π	2.1(1)% at E_γ = 1408 keV	4 MeV	2.5(1)% at E_γ = 1408 keV	320(5) ps
Hybrid array at TRIUMF [36]	9 detectors from FATIMA	planar	4.48(1)% at E_γ = 1332 keV ($LaBr_3$(Ce) only)	11 MeV	–	538 ps
Array at NSCL [37]	16 pc 1.5″ × 1.5″	planar	1.9% at E_γ = 1332 keV	3 MeV	2.8% at E_γ = 1836.1 keV	310 ps
ROSPHERE at IFIN-HH [38]	19 pc 1.5″ × 1.5″, 2″ × 2″	4 π	–	2 MeV	1.75(5)% at E_γ = 1332 keV (11 detectors)	347(10) ps
NANA at UK NPL [39], [40]	8 from FATIMA	planar	3% at E_γ = 1332 keV	2.5 MeV	–	–
ν-ball [41]	20 pc 1.5″ × 2″, 1″ × 1.5″ × 2″	planar	3 and 2.7% at E_γ = 662 keV	11 MeV	1.4% at E_γ = 1 MeV[1]	210 ps, 160 ps
OSCAR at Oslo [42]	30 pc 3.5″ × 8″	57% of 4π	–	–	2.54% at E_γ = 1332 keV	–
γ^3 at HIγS [43]	8 pc 1.5″ × 1.5″, 3″ × 3″	4π	–	3.2 MeV	6% at E_γ = 1332 keV	–
Array at RIKEN [44]	18 pc 1.5″ × 2″	planar	10% at E_γ = 150–170 keV	1.3 MeV	4% at E_γ = 150-170 keV	825(25) ps
Array at iTHEMBA [45]	8 pc 2″ × 2″	planar	3.19% at E_γ = 1332 keV	1.3 MeV	2.8% at E_γ = 1332 keV	372(3) ps[2]
ELIGANT-GN [29]	15 pc 2″ × 2″	2 π	3.54% at E_γ = 662 keV[3]	20 MeV	1.22% at E_γ = 662 keV	387 ps
Array coupled to GALILEO at LNL [46,47]	10 pc 3″ × 3″	planar	3% at E_γ = 662 keV[3]	16 MeV	2.3% at E_γ = 1332 keV	700–850 ps

[1] From GEANT4 simulation
[2] Calculated from [45]
[3] Calculated from [29].

resolution is also competitive with that of similar arrays employing smaller crystals. Characteristics of some planned arrays with similar size $LaBr_3$(Ce) detectors can be found in Refs. [31–33]. A comprehensive and detailed review of $LaBr_3$(Ce) detector systems is beyond the scope of this paper.

To facilitate the use of the LABDA detector system, we conducted two in-beam measurements: one for nuclear astrophysics and one for nuclear technology applications.

6.1. The ^{14}N(p, γ)^{15}O reaction

Accurate knowledge of the reactions in the carbon–nitrogen–oxygen (CNO) cycle is essential for comparing the predictions of the Standard Solar Model [48], which provides a complex description of the Sun with solar neutrino observations [49]. Furthermore, understanding the CNO cycle is important for the theoretical calibration of globular cluster ages as a tool to estimate the age of the Universe [50]. The ^{14}N(p, γ)^{15}O reaction with a Q value of 7296.8 keV plays a fundamental role in the CNO cycle, acting as its bottleneck [18,51]. The reaction rate at stellar temperatures is affected by transitions through numerous excited states and the ground state of ^{15}O. The nuclear properties of the reaction, such as the branching ratios and resonance strengths, are crucial for low-energy extrapolation.

Solid state TiN targets were prepared by reactive sputtering of TiN onto 0.5 mm thick Ta backings at the Helmholtz-Zentrum Dresden-Rossendorf, Germany. The nominal thickness of the TiN layers was about 300 nm, corresponding to roughly 1.5 × 10^{18} N atoms/cm^2. Target properties such as Ti:N ratio (0.976 ± 0.048), target thickness ($\Delta E = 24.4 \pm 1$ keV) and test of the presence of impurities are described in Ref. [18].

The LABDA array was used to measure the resonance strength ($\omega\gamma$) of the E_p = 1058 keV resonance as well as the branching ratios (B^i) for

Table 3
Resonance strength and branching ratios of E_{res} = 1058 keV resonance of ^{14}N(p, γ)^{15}O reaction.

Transitions	E_γ (keV)	ωγ (eV)	Branching Ratio (%)
DC→0	8284	0.39 ± 0.06	52 ± 2
5241→0	5241	0.41 ± 0.06	44 ± 2
DC→5241	3042	0.39 ± 0.06	44 ± 2

DC→0, DC→5241 and 5241→0 transitions using the following formula:

$$\omega\gamma = \frac{2\epsilon_{\rm eff}(E)A_\gamma(E)}{\lambda^2 B^i N_p \eta_{eff} f} \quad , \tag{4}$$

where A_γ is the area of the detected γ-ray peak at proton energy E of a given transitions measured in the middle of the resonance curve plateau, $\epsilon_{\rm eff}(E)$ is the effective stopping power (15.59 eV/10^{15} atoms/cm^2) and λ is the de Broglie wavelength at the resonance energy in the center-of-mass system. N_p is the number of bombarding particles and f = 0.902 ± 0.02 is a correction factor to obtain the yield related to an ideal thick target using Eq. 4.102. in Ref. [21]. As the parameters of the weak transitions could not be derived from our data due to the low η_{eff} in the experimental geometry, B^i of the weak transitions (6859→ 0, 6172 →0 and 5181→0) were taken from Ref. [52].

The results obtained as the average of the data measured with 12 detectors at θ = 41.97° and 78.69° are shown in Table 3. The uncertainties were calculated as a quadratic sum of statistical uncertainties (≤4%) and the contributions from the target properties (∼4.5%), N_p (∼3%), normalization of the η_{eff} (∼10%) and background subtractions (∼8%) (See Sections 4 and 3.2).

The resonance strengths derived from the study of different transitions are consistent with literature data of 0.364 ± 0.021 eV obtained in

Table 4
The level parameters (level energies, spin-parity), final state of transitions, neutron energies of different neutron groups and the calculated branching ratios at E_p = 3000 keV.

E_x (level) [keV]; J^π	E_γ [keV]; I (%)	Final state [keV]	n group; E_n [keV]	Branching ratio (%)	
				Present	Talys
0; 7/2-			n_0; 1408	**68.8** ± **1.5**	65
749.1; 3/2-	749; 100	0	n_1; 660	**8.1** ± **0.5**	11
776.95[a]; 1/2-	27.84; 100	749.1	n_2; 660		
	776.95; ≤0.6	0			
1164.59; 9/2-	1164.5; 100	0	n_3; 244	**17.1** ± **0.9**	18
1352.65; 5/2-	575.6; 16	776.95	n_4; 56	**6.0** ± **0.4**	6
	603.5; 100	749.1			
	1353.7; 61.5	0			

[a] The 776.95 keV transition mainly leads to the state at E_x = 749.1 keV which decays to the ground state by the 749 keV transition, and thus the two γ rays cannot be separated from each other.

an in-beam measurement [52], and with the value of 0.442 ± 0.024 eV reported using the activation methods [18].

6.2. The ^{51}V(p,n)^{51}Cr reaction

The ^{51}V(p,n)^{51}Cr reaction is widely used in many fields of physics, *e.g.* in medical diagnostics [53], in the study of material loss using the Thin Layer Activation Technique [54], and as a monoenergetic neutron source for detector calibration [55]. The energy and flux of the emitted neutrons can be easily controlled using a proton beam above the reaction threshold (E_p ~1565 keV). The total number of emitted neutrons (N_{total}) can be determined by measuring the number of ^{51}Cr radioactive nuclei produced by the reaction via the activation technique. However, its application is limited to E_p ≤2300 keV (equivalent to E_n ~700 keV) due to the opening of additional neutron channels corresponding to the first and higher excited states of ^{51}Cr. As a result, neutrons with different energies (n_0 for the ground state transition, n_1 for the first excited state at E_X = 749 keV, etc.) may be present in the emitted neutron spectrum of the reaction.

To extend the application of this reaction to higher neutron energies, a target of ^{nat}V evaporated onto a 0.25 mm thick tantalum backing was prepared and irradiated at E_p = 3000 keV at the Tandetron accelerator. The nominal thickness of the vanadium layer was around 345 nm, corresponding roughly to 2.5 × 10^{18} ^{nat}V atoms/cm^2.

The E_γ = 576, 604, 749, 1165 and 1354 keV lines were analyzed to calculate the branching ratios of n_{0-4} neutron groups at E_p = 3000 keV. The level parameters and the calculated branching ratios are summarized in Table 4. To support the experimental analysis, γ branching ratios were modeled, using the open access *TALYS 1.97* nuclear reaction code [56] based on different nuclear structure models.

The measured and the calculated ratios of E_x = 0 and 749 keV transitions differ at the few percent level, likely due to the γ rays from the ^{51}V(n,n')^{51}V reaction contributing to the studied γ transitions, a consequence of the limited energy resolution of the scintillators. Nevertheless, the new results allow us to extend the application of the ^{51}V(p,n)^{51}Cr reaction for detector calibration up to E_n ~1500 keV completed by simulations of the experimental setup. We noted here that a comprehensive study of this reaction in the 1300–1900 keV range, using the LABDA array with a wider detection angle, is ongoing.

6.3. Summary and outlook

Recently, a LaBr$_3$(Ce) γ-spectrometer, the LABDA array, was designed and installed at HUN-REN ATOMKI, Debrecen, Hungary. The energy resolution, energy non-linearity, and the detection efficiency of the setup were characterized over the 344–10762 keV γ-ray energy range. The performance of the array was modeled using GEANT4 simulations, and the impact of Compton background on peak area determination was evaluated. To reduce the intrinsic α-background of the detectors, different pulse shape discrimination methods were tested. To facilitate the use of the detector system for nuclear physics and nuclear technology application experiments, two commissioning measurements were performed. We obtained the resonance strength of ^{14}N(p, γ)^{15}O reaction at E_r = 1058 keV agreeing with in-beam and activation experiments, and determined the branching ratios of ^{51}V(p,n)^{51}Cr reaction extend its application as a neutron source to E_n = 1500 keV. A more comprehensive study of the ^{51}V(p,n)^{51}Cr reaction over the E_n = 130–1900 keV range, using the LABDA array with an extended detection angle coverage, is currently in progress. Moreover, in the near future, a new detector configuration combined with a high intensity beamline (I≥ 20 μA of $^+$H) at the Tandetron accelerator is expected to increase the detection efficiency by a factor of 100, while also improving the angular resolution of the setup. This will enable high-precision measurements of nuclear parameters of high Q-value reactions (e.g. ^{12,13}C(p, γ)^{13,14}N, ^{14}N(p, γ)^{15}O and ^{17}O(p, γ)^{18}F), including the weak transitions, over a wide energy range, thereby enhancing the reliability of low energy extrapolations and revealing astrophysical phenomena connected to, e.g. the CNO cycle in various astrophysical sites.

CRediT authorship contribution statement

L. Csedreki: Writing – review & editing, Writing – original draft, Visualization, Validation, Supervision, Project administration, Formal analysis, Data curation, Conceptualization. **M. Begala:** Writing – original draft, Software, Methodology, Formal analysis. **M.M. Juhász:** Writing – original draft, Visualization, Validation, Formal analysis. **D. Sohler:** Writing – original draft, Project administration, Methodology, Conceptualization. **Z. Elekes:** Writing – original draft, Software, Formal analysis, Data curation. **A.J. Krasznahorkay:** Writing – original draft, Project administration, Funding acquisition.

Declaration of competing interest

The authors declare that they have no known competing financial interests or personal relationships that could have appeared to influence the work reported in this paper.

Acknowledgments

This work was supported by the HUN-REN Office for Supported Research Groups (TKI), Hungary under the Award No. TKCS-2024/56 (project ID: 3510217), by the National Research, Development and Innovation Fund of Hungary (NKFIH) financed by projects with contract no. TKP2021-NKTA-42, GINOP-2.3.3-15-456-2016-00005 and GINOP-2.3.3-15-2016-00034. L. Cs. acknowledges the support of the János Bolyai Reserach Scholarship of the Hungarian Academy of Science. M.B. was supported by the EKÖP-25-3 University Research Scholarship Program of the Ministry for Culture and Innovation from the source of the National Research, Development and Innovation Fund.

We acknowledge the support of G. Gy. Kiss in writing and editing the paper.

Data availability

Data will be made available on request.

References

[1] Saint-gobain crystals, France, data sheet of material BrilLanCe 380, 1948.

[2] E. van Loef, P. Dorenbos, C. van Eijk, K. Krämer, H. Güdel, Scintillation properties of $LaBr_3:Ce^{3+}$ crystals: fast, efficient and high-energy-resolution scintillators, Nucl. Instrum. Methods Phys. Res. Sect. A: Accel. Spectrometers, Detect. Assoc. Equip. 486 (1) (2002) 254–258, Proceedings of the 6th International Conference on Inorganic Scin tillators and their Use in Scientific and Industrial Applications.

[3] M. Moszyński, A. Nassalski, A. Syntfeld-Każuch, T. Szczęśniak, W. Czarnacki, D. Wolski, G. Pausch, J. Stein, Temperature dependences of $LaBr_3$(Ce), $LaCl_3$(Ce) and NaI(Tl) scintillators, Nucl. Instrum. Methods Phys. Res. Sect. A: Accel. Spectrometers, Detect. Assoc. Equip. 568 (2) (2006) 739–751.

[4] M. Ciemala, D. Balabanski, M. Csatlos, J. Daugas, G. Georgiev, J. Gulyas, M. Kmiecik, A. Krasznahorkay, S. Lalkovski, A. Lefebvre-Schuhl, R. Lozeva, A. Maj, A. Vitez, Measurements of high-energy γ-rays with $LaBr_3$:Ce detectors, Nucl. Instrum. Methods Phys. Res. Sect. A, Accel. Spectrometers, Detect. Assoc. Equip. 608 (1) (2009) p. 76–79.

[5] Y.A. Trofimov, E.E. Lupar, V.N. Yurov, Linearity of the energy scale of a detector based on a $LaBr_3$:(Ce) scintillator, Instrum. Exp. Tech. 56 (2013) p. 151–155.

[6] D. Weisshaar, M. Wallace, P. Adrich, D. Bazin, C. Campbell, J. Cook, S. Ettenauer, A. Gade, T. Glasmacher, S. McDaniel, A. Obertelli, A. Ratkiewicz, A. Rogers, K. Siwek, S. Tornga, $LaBr_3$:Ce scintillators for in-beam gamma-ray spectroscopy with fast beams of rare isotopes, Nucl. Instrum. Methods Phys. Res. Sect. A: Accel. Spectrometers, Detect. Assoc. Equip. 594 (1) (2008) 56–60.

[7] J. Kiener, V. Tatischeff, I. Deloncle, N. de Séréville, P. Laurent, C. Blondel, M. Chabot, R. Chipaux, A. Coc, S. Dubos, A. Gostojic', N. Goutev, C. Hamadache, F. Hammache, B. Horeau, O. Limousin, S. Ouichaoui, G. Prévot, R. Rodríguez-Gasén, M. Yavahchova, Fast-neutron induced background in $LaBr_3$:Ce detectors, Nucl. Instrum. Methods Phys. Res. Sect. A: Accel. Spectrometers, Detect. Assoc. Equip. 798 (2015) 152–161.

[8] A. Lavagno, G. Gervino, A. Scarfone, Study of linearity and internal background for $LaBr_3$(Ce) γ-ray scintillation detector, Nucl. Instrum. Methods Phys. Res. Sect. A: Accel. Spectrometers, Detect. Assoc. Equip. 718 (2013) 504–505, Proceedings of the 12th Pisa Meeting on Advanced Detectors.

[9] H. Cheng, B.H. Sun, L.H. Zhu, T.X. Li, G.S. Li, C.B. Li, X.G. Wu, Y. Zheng, Intrinsic background radiation of $LaBr_3$(Ce) detector via coincidence measurements and simulations, Nucl. Sci. Tech. 31 (99) (2020) 1–10.

[10] E. Khilkevitch, A. Shevelev, I. Chugunov, M. Iliasova, D. Doinikov, D. Gin, V. Naidenov, I. Polunovsky, Advanced algorithms for signal processing scintillation gamma ray detectors at high counting rates, Nucl. Instrum. Methods Phys. Res. Sect. A: Accel. Spectrometers, Detect. Assoc. Equip. 977 (2020) 164309.

[11] M. Zeng, J. Cang, Z. Zeng, X. Yue, J. Cheng, Y. Liu, H. Ma, J. Li, Quantitative analysis and efficiency study of PSD methods for a $LaBr_3$:Ce detector, Nucl. Instrum. Methods Phys. Res. Sect. A: Accel. Spectrometers, Detect. Assoc. Equip. 813 (2016) 56–61.

[12] T. Alharbi, Rejection of the internal α background in $LaBr_3$(Ce) detectors by using a wavelet-based pulse-shape discrimination method, J. King Saud Univ. – Sci. 34 (2019) 101925.

[13] A.J. Krasznahorkay, M. Csatlós, L. Csige, Z. Gácsi, J. Gulyás, M. Hunyadi, I. Kuti, B.M. Nyakó, L. Stuhl, J. Timár, T.G. Tornyi, Z. Vajta, T.J. Ketel, A. Krasznahorkay, Observation of anomalous internal pair creation in ^{8}Be: A possible indication of a light, neutral boson, Phys. Rev. Lett. 116 (2016) 042501.

[14] A. Nagy, A.J. Krasznahorkay, M. Ciemala, M. Csatlós, L. Csige, Z. Gácsi, M. Hunyadi, T. Klaus, M. Kmiecik, A. Maj, N. Pietralla, Z. Révay, N. Sas, C. Stieghorst, J. Timár, T. Tornyi, Searching for the double gamma-decay of the X(17) particle, Nuovo Cimento C- Colloq. Commun. Phys. 42 C (124) (2019) 1–4.

[15] A. Giaz, L. Pellegri, S. Riboldi, F. Camera, N. Blasi, C. Boiano, A. Bracco, S. Brambilla, S. Ceruti, S. Coelli, F. Crespi, M. Csatlòs, S. Frega, J. Gulyàs, A. Krasznahorkay, S. Lodetti, B. Million, A. Owens, F. Quarati, L. Stuhl, O. Wieland, Characterization of large volume $3.5'' \times 8''$ $LaBr_3$:Ce detectors, Nucl. Instrum. Methods Phys. Res. Sect. A: Accel. Spectrometers, Detect. Assoc. Equip. 729 (2013) 910–921.

[16] A. Antilla, J. Keinonen, M. Hautala, I. Forsblom, Use of the $^{27}Al(p,\gamma)^{28}Si$, E_p=992 keV resonance as a gamma-ray intensity standard, Nucl. Instrum. Methods 147 (3) (1977) 501–505.

[17] I. Rajta, I. Vajda, G. Gyürky, L. Csedreki, Á.Z. Kiss, S. Biri, H.A.P. van Oosterhout, N.C. Podaru, D.J.W. Mous, Accelerator characterization of the new ion beam facility at MTA Atomki in Debrecen, Hungary, Nucl. Instrum. Methods Phys. Res. A 880 (2018) 125–130.

[18] G. Gyürky, Z. Halász, G. Kiss, T. Szücs, A. Csík, Z. Török, R. Huszánk, M. Kohan, L. Wagner, Z. Fülöp, Resonance strengths in the $^{14}N(p,\gamma)^{15}O$ astrophysical key reaction measured with activation, Phys. Rev. C 100 (1) (2019).

[19] V.T. Jordanov, G.F. Knoll, Digital synthesis of pulse shapes in real time for high resolution radiation spectroscopy, Nucl. Instrum. Methods Phys. Res. Sect. A: Accel. Spectrometers, Detect. Assoc. Equip. 345 (2) (1994) 337–345.

[20] A. Owens, A. Bos, S. Brandenburg, C. Dathy, P. Dorenbos, S. Kraft, R. Ostendorf, V. Ouspenski, F. Quarati, γ-Ray performance of a 1242 cm^3 $LaCl_3$:Ce scintillation spectrometer, Nucl. Instrum. Methods Phys. Res. Sect. A: Accel. Spectrometers, Detect. Assoc. Equip. 574 (1) (2007) 110–114.

[21] C. Iliadis, Nuclear Physics of Stars, Wiley-VCH, 2008.

[22] M.E. Rose, The analysis of angular correlation and angular distribution data, Phys. Rev. 91 (1953) 610–615.

[23] S.O. Flyckt, C. Marmonier, Photomultiplier tubes, Photonis, Brive, 2002.

[24] G. Knoll, Radiation Detection and Measurement, John Wiley & Sons, Inc., New York, 1989.

[25] S. Agostinelli, J. Allison, K. Amako, J. Apostolakis, H. Araujo, P. Arce, M. Asai, D. Axen, S. Banerjee, G. Barrand, F. Behner, L. Bellagamba, J. Boudreau, L. Broglia, A. Brunengo, H. Burkhardt, S. Chauvie, J. Chuma, R. Chytracek, G. Cooperman, G. Cosmo, P. Degtyarenko, A. Dell'Acqua, G. Depaola, D. Dietrich, R. Enami, A. Feliciello, C. Ferguson, H. Fesefeldt, G. Folger, F. Foppiano, A. Forti, S. Garelli, S. Giani, R. Giannitrapani, D. Gibin, J. Gómez Cadenas, I. González, G. Gracia Abril, G. Greeniaus, W. Greiner, V. Grichine, A. Grossheim, S. Guatelli, P. Gumplinger, R. Hamatsu, K. Hashimoto, H. Hasui, A. Heikkinen, A. Howard, V. Ivanchenko, A. Johnson, F. Jones, J. Kallenbach, N. Kanaya, M. Kawabata, Y. Kawabata, M. Kawaguti, S. Kelner, P. Kent, A. Kimura, T. Kodama, R. Kokoulin, M. Kossov, H. Kurashige, E. Lamanna, T. Lampén, V. Lara, V. Lefebure, F. Lei, M. Liendl, W. Lockman, F. Longo, S. Magni, M. Maire, E. Medernach, K. Minamimoto, P. Mora de Freitas, Y. Morita, K. Murakami, M. Nagamatu, R. Nartallo, P. Nieminen, T. Nishimura, K. Ohtsubo, M. Okamura, S. O'Neale, Y. Oohata, K. Paech, J. Perl, A. Pfeiffer, M. Pia, F. Ranjard, A. Rybin, S. Sadilov, E. Di Salvo, G. Santin, T. Sasaki, N. Savvas, Y. Sawada, S. Scherer, S. Sei, V. Sirotenko, D. Smith, N. Starkov, H. Stoecker, J. Sulkimo, M. Takahata, S. Tanaka, E. Tcherniaev, E. Safai Tehrani, M. Tropeano, P. Truscott, H. Uno, L. Urban, P. Urban, M. Verderi, A. Walkden, W. Wander, H. Weber, J. Wellisch, T. Wenaus, D. Williams, D. Wright, T. Yamada, H. Yoshida, D. Zschiesche, Geant4—a simulation toolkit, Nucl. Instrum. Methods Phys. Res. Sect. A: Accel. Spectrometers, Detect. Assoc. Equip. 506 (3) (2003) 250–303.

[26] R. Scafè, R. Pani, R. Pellegrini, M.N. Cinti, P. Bennati, S. Lo Meo, MgO reflectance data for Monte Carlo simulation of $LaBr_3$:Ce scintillation crystals, Nucl. Instrum. Methods Phys. Res. Sect. A: Accel. Spectrometers, Detect. Assoc. Equip. 701 (2013) 44–53.

[27] J. Allison, K. Amako, J. Apostolakis, P. Arce, M. Asai, T. Aso, E. Bagli, A. Bagulya, S. Banerjee, G. Barrand, B. Beck, A. Bogdanov, D. Brandt, J. Brown, H. Burkhardt, P. Canal, D. Cano-Ott, S. Chauvie, K. Cho, G. Cirrone, G. Cooperman, M. Cortés-Giraldo, G. Cosmo, G. Cuttone, G. Depaola, L. Desorgher, X. Dong, A. Dotti, V. Elvira, G. Folger, Z. Francis, A. Galoyan, L. Garnier, M. Gayer, K. Genser, V. Grichine, S. Guatelli, P. Guèye, P. Gumplinger, A. Howard, I. Hřivnáčová, S. Hwang, S. Incerti, A. Ivanchenko, V. Ivanchenko, F. Jones, S. Jun, P. Kaitaniemi, N. Karakatsanis, M. Karamitros, M. Kelsey, A. Kimura, T. Koi, H. Kurashige, A. Lechner, S. Lee, F. Longo, M. Maire, D. Mancusi, A. Mantero, E. Mendoza, B. Morgan, K. Murakami, T. Nikitina, L. Pandola, P. Paprocki, J. Perl, I. Petrović, M. Pia, W. Pokorski, J. Quesada, M. Raine, M. Reis, A. Ribon, A. Ristić Fira, F. Romano, G. Russo, G. Santin, T. Sasaki, D. Sawkey, J. Shin, I. Strakovsky, A. Taborda, S. Tanaka, B. Tomé, T. Toshito, H. Tran, P. Truscott, L. Urban, V. Uzhinsky, J. Verbeke, M. Verderi, B. Wendt, H. Wenzel, D. Wright, D. Wright, T. Yamashita, J. Yarba, H. Yoshida, Recent developments in Geant4, Nucl. Instrum. Methods Phys. Res. Sect. A: Accel. Spectrometers, Detect. Assoc. Equip. 835 (2016) 186–225.

[28] R. Nicolini, F. Camera, N. Blasi, S. Brambilla, R. Bassini, C. Boiano, A. Bracco, F. Crespi, O. Wieland, G. Benzoni, S. Leoni, B. Million, D. Montanari, A. Zalite, Investigation of the properties of a $1''\times1''$ $LaBr_3$:Ce scintillator, Nucl. Instrum. Methods Phys. Res. Sect. A: Accel. Spectrometers, Detect. Assoc. Equip. 582 (2) (2007) 554–561.

[29] P.-A. Söderström, E. Açıksöz, D. Balabanski, F. Camera, L. Capponi, G. Ciocan, M. Cuciuc, D. Filipescu, I. Gheorghe, T. Glodariu, J. Kaur, M. Krzysiek, C. Matei, T. Roman, A. Rotaru, A. Şerban, A. State, H. Utsunomiya, V. Vasilca, ELIGANT-GN — ELI Gamma above neutron threshold: The Gamma-neutron setup, Nucl. Instrum. Methods Phys. Res. Sect. A: Accel. Spectrometers, Detect. Assoc. Equip. 1027 (2022) 166171.

[30] F. Crespi, F. Camera, N. Blasi, A. Bracco, S. Brambilla, B. Million, R. Nicolini, L. Pellegri, S. Riboldi, M. Sassi, O. Wieland, F. Quarati, A. Owens, Alpha–gamma discrimination by pulse shape in $LaBr_3$:Ce and $LaCl_3$:Ce, Nucl. Instrum. Methods Phys. Res. Sect. A: Accel. Spectrometers, Detect. Assoc. Equip. 602 (2) (2009) 520–524.

[31] M. Krzysiek, F. Camera, D. Filipescu, H. Utsunomiya, G. Colò, I. Gheorghe, Y. Niu, Simulation of the ELIGANT-GN array performances at ELI-NP for gamma beam energies larger than neutron threshold, Nucl. Instrum. Methods Phys. Res. Sect. A: Accel. Spectrometers, Detect. Assoc. Equip. 916 (2019) 257–274.

[32] A. Tamii, L. Pellegri, P.-A. Söderström, D. Allard, S. Goriely, T. Inakura, E. Khan, E. Kido, M. Kimura, E. Litvinova, S. Nagataki, P. von Neumann-Cosel, N. Pietralla, N. Shimizu, N. Tsoneva, Y. Utsuno, S. Adachi, P. Adsley, A. Bahini, D. Balabanski, B. Baret, J.A.C. Bekker, S.D. Binda, E. Boicu, A. Bracco, I. Brandherm, M. Brezeanu, J.W. Brummer, F. Camera, F.C.L. Crespi, R. Dalal, L.M. Donaldson, Y. Fujikawa, T. Furuno, H. Haoning, R. Higuchi, Y. Honda, A. Gavrilescu, A. Inoue, J. Isaak, H. Jivan, P. Jones, S. Jongile, O. Just, T. Kawabata, T. Khumalo, J. Kiener, J. Kleemann, N. Kobayashi, Y. Koshio, A. Kuşoğlu, K.C.W. Li, K.L. Malatji, R.E. Molaeng, H. Motoki, M. Murata, A.A. Netshiya, R. Neveling, R. Niina, S. Okamoto, S. Ota, O. Papst, E. Parizot, T. Petruse, M.S. Reen, P. Ring, K. Sakanashi, E. Sideras-Haddad, S. Siem, M. Spall, T. Suda, T. Sudo, Y. Taniguchi, V. Tatischeff, H. Utsunomiya, H. Wang, V. Werner, H. Wibowo, M. Wiedeking, O. Wieland, Y. Xu, Z.H. Yang, PANDORA Collaboration, PANDORA project for the study of photonuclear reactions below $A = 60$, Eur. Phys. J. A 59 (9) (2023) 208.

[33] J. Valiente-Dobón, R. Menegazzo, A. Goasduff, D. Agguiaro, P. Aguilera, F. Angelini, M. Balogh, D. Bazzacco, J. Benito, G. Benzoni, N. Bez, M. Bolognesi, S. Bottoni, D. Brugnara, S. Carollo, P. Cocconi, A. Cogo, J. Collado, F. Crespi, A. Ertoprak, R. Escudeiro, F. Galtarossa, E. Gamba, A. Gambalonga, B.G. Servín, A. Gottardo, A. Gozzelino, M. Gulmini, Z. Huang, T. Marchi, D. Mengoni, P. Modanese, D. Napoli, J. Pellumaj, R. Pérez-Vidal, S. Pigliapoco, E. Pilotto, L. Ramina, M. Rampazzo, W. Raniero, M. Rebeschini, K. Rezynkina, D. Rosso, M. Scarcioffolo, D. Scarpa, M. Sedlák, R. Smith, N. Toniolo, F. Veronese, V. Volpe, L. Zago, I. Zanon, G. Zhang, R. Abels, M. Allegrini, C. Aufranc, G. Baulieu, C. Belkhiria, M. Benettoni, D. Benini, M. Bentley, M. Biasotto, M. Blaizot, J.B. Miquel, C. Boiano, A. Boston, H. Boston, A. Boujrad, P. Bourgault, A. Bracco, S. Brambilla, I. Burrows, F. Camera, S. Capra, A. Capsoni, R. Cash, J. Civera, E. Clément, S. Coelli, M. Cordwell, L. Corradi, S. Coudert, G. De Angelis, L. De Ruvo, G. Debras, M. Del Fabbro, J. Diklić, N. Dosme, G. Duchene, B. Duclos, J. Dudouet, J. Eberth, S. Elloumi, C. Everett, S. Fantinel, M. Fillinger, E. Fioretto, C. Fransen, A. Gadea, L. Gibelin, V. González, J. Goupil, C. Görgen, A. Grant, K. Green, J. Ha, T. Hartnett, K. Henseler, H. Hess, R. Hirsch, C. Houarner, J. Jacob, T. Joannem, D. Judson, N. Karkour, M. Karolak, M. Kebbiri, J. Kieffer, M. Labiche, X. Lafay, P. Le Jeannic, A. Lefevre, E. Legay, F. Legruel, S. Lenzi, S. Leoni, D. Linget, M. Liptrot, A. López-Martens, A. Lotodé, L. Manara, L. Ménager, T. Mijatović, B. Million, A. Minarello, G. Montagnoli, P. Morrall, I. Mullacrane, J. Nyberg, G. Philippon, M. Polettini, F. Popieul, A. Pullia, F. Recchia, P. Reiter, G. Richardt, M. Rocchini, A. Roger, F. Saillant, E. Sanchis, M. Laskar, G. Secci, M.-H. Sigward, J. Simpson, N. Solenne, F. Spee, A. Stefanini, O. Stézowski, S. Szilner, N. Templeton, C. Theisen, S. Thiel, F. Tomasi, S. Tzvetkov, D. Vigano, E. Viscione, O. Wieland, K. Wimmer, G. Wittwer, M. Zielińska, Conceptual design of the AGATA 2π array at LNL, Nucl. Instrum. Methods Phys. Res. Sect. A: Accel. Spectrometers, Detect. Assoc. Equip. 1049 (2023) 168040.

[34] O.J. Roberts, A.M. Bruce, P.H. Regan, Z. Podolyák, C.M. Townsley, J.F. Smith, K.F. Mulholland, A. Smith, A $LaBr_3$:Ce fast-timing array for DESPEC at FAIR, Nucl. Instrum. Methods Phys. Res. Sect. A: Accel. Spectrometers, Detect. Assoc. Equip. 748 (2014) 91–95.

[35] M. Rudigier, Z. Podolyák, P. Regan, A. Bruce, S. Lalkovski, R. Canavan, E. Gamba, O. Roberts, I. Burrows, D. Cullen, L. Fraile, L. Gerhard, J. Gerl, M. Gorska, A. Grant, J. Jolie, V. Karayonchev, N. Kurz, W. Korten, I. Lazarus, C. Nita, V. Pucknell, J.-M. Régis, H. Schaffner, J. Simpson, P. Singh, C. Townsley, J. Smith, J. Vesic, FATIMA — FAst TIMing array for DESPEC at FAIR, Nucl. Instrum. Methods Phys. Res. Sect. A: Accel. Spectrometers, Detect. Assoc. Equip. 969 (2020) 163967.

[36] G. Christian, D. Hutcheon, I. Casandjian, S. Collins, A. Edwin, E. Desmarais, U. Greife, A. Katrusiak, A. Lennarz, M. Loria, S. Molló, J. O'Connell, S. Pascu, L. Pedro-Botet, Z. Podolyák, B. Reed, P. Regan, C. Ruiz, R. Shearman, S. Upadhyayula, L. Wagner, M. Williams, First in-beam demonstration of a hybrid $LaBr_3$/$CeBr_3$/BGO array to measure radiative capture resonance energies in an extended gas target using a novel time of flight technique, Nucl. Instrum. Methods Phys. Res. Sect. A: Accel. Spectrometers, Detect. Assoc. Equip. 1072 (2025) 170199.

[37] B. Longfellow, P. Bender, J. Belarge, A. Gade, D. Weisshaar, Commissioning of the $LaBr_3$(Ce) detector array at the National Superconducting Cyclotron Laboratory, Nucl. Instrum. Methods Phys. Res. Sect. A: Accel. Spectrometers, Detect. Assoc. Equip. 916 (2019) 141–147.

[38] D. Bucurescu, I. Căta-Danil, G. Ciocan, C. Costache, D. Deleanu, R. Dima, D. Filipescu, N. Florea, D. Ghiţă, T. Glodariu, M. Ivaşcu, R. Lică, N. Mărginean, R. Mărginean, C. Mihai, A. Negret, C. Niţă, A. Olăcel, S. Pascu, T. Sava, L. Stroe, A. Şerban, R. Şuvăilă, S. Toma, N. Zamfir, G. Căta-Danil, I. Gheorghe, I. Mitu, G. Suliman, C. Ur, T. Braunroth, A. Dewald, C. Fransen, A. Bruce, Z. Podolyák, P. Regan, O. Roberts, The ROSPHERE γ-ray spectroscopy array, Nucl. Instrum. Methods Phys. Res. Sect. A: Accel. Spectrometers, Detect. Assoc. Equip. 837 (2016) 1–10.

[39] R. Shearman, S. Collins, G. Lorusso, M. Rudigier, S. Judge, S. Bell, Z. Podolyak, P. Regan, Commissioning of the UK national nuclear array, Radiat. Phys. Chem. 140 (2017) 475–479, 2nd International Conference on Dosimetry and its Applications (ICDA-2) University of Surrey, Guildford, United Kingdom, 3-8 July 2016.

[40] S. Collins, R. Shearman, J. Keightley, P. Regan, Investigation of $\gamma-\gamma$ coincidence counting using the national nuclear array (NANA) as a primary standard, Appl. Radiat. Isot. 134 (2018) 290–296, ICRM 2017 Proceedings of the 21st International Conference on Radionuclide Metrology and its Applications.

[41] M. Lebois, N. Jovančević, D. Thisse, R. Canavan, D. Étasse, M. Rudigier, J. Wilson, The ν-ball γ-spectrometer, Nucl. Instrum. Methods Phys. Res. Sect. A: Accel. Spectrometers, Detect. Assoc. Equip. 960 (2020) 163580.

[42] F. Zeiser, G. Tveten, F. Bello Garrote, M. Guttormsen, A. Larsen, V. Ingeberg, A. Görgen, S. Siem, The γ-ray energy response of the oslo scintillator array OSCAR, Nucl. Instrum. Methods Phys. Res. Sect. A: Accel. Spectrometers, Detect. Assoc. Equip. 985 (2021) 164678.

[43] B. Löher, V. Derya, T. Aumann, J. Beller, N. Cooper, M. Duchêne, J. Endres, E. Fiori, J. Isaak, J. Kelley, M. Knörzer, N. Pietralla, C. Romig, D. Savran, M. Scheck, H. Scheit, J. Silva, A. Tonchev, W. Tornow, H. Weller, V. Werner, A. Zilges, The high-efficiency γ-ray spectroscopy setup γ^3 at HIγS, Nucl. Instrum. Methods Phys. Res. Sect. A: Accel. Spectrometers, Detect. Assoc. Equip. 723 (2013) 136–142.

[44] F. Browne, A. Bruce, T. Sumikama, I. Nishizuka, S. Nishimura, P. Doornenbal, G. Lorusso, P.-A. Söderström, H. Watanabe, R. Daido, Z. Patel, S. Rice, L. Sinclair, J. Wu, Z. Xu, A. Yagi, H. Baba, N. Chiga, R. Carroll, F. Didierjean, Y. Fang, N. Fukuda, G. Gey, E. Ideguchi, N. Inabe, T. Isobe, D. Kameda, I. Kojouharov, N. Kurz, T. Kubo, S. Lalkovski, Z. Li, R. Lozeva, H. Nishibata, A. Odahara, Z. Podolyák, P. Regan, O. Roberts, H. Sakurai, H. Schaffner, G. Simpson, H. Suzuki, H. Takeda, M. Tanaka, J. Taprogge, V. Werner, O. Wieland, Lifetime measurements of the first 2^+ states in ^{104,106}Zr: Evolution of ground-state deformations, Phys. Lett. B 750 (2015) 448–452.

[45] L. Msebi, V. Ingeberg, P. Jones, J. Sharpey-Schafer, A. Avaa, T. Bucher, C. Brits, M. Chisapi, D. Kenfack, E. Lawrie, K. Malatji, B. Maqabuka, L. Makhathini, S. Noncolela, J. Ndayishimye, A. Netshiya, O. Shrinda, M. Wiedeking, B. Zikhali, A fast-timing array of 2'' x 2'' $LaBr_3$:Ce detectors for lifetime measurements of excited nuclear states, Nucl. Instrum. Methods Phys. Res. Sect. A: Accel. Spectrometers, Detect. Assoc. Equip. 1026 (2022) 166195.

[46] A. Goasduff, D. Mengoni, F. Recchia, J. Valiente-Dobón, R. Menegazzo, G. Benzoni, D. Barrientos, M. Bellato, N. Bez, M. Biasotto, N. Blasi, C. Boiano, A. Boso, S. Bottoni, A. Bracco, S. Brambilla, D. Brugnara, F. Camera, S. Capra, A. Capsoni, P. Cocconi, S. Coelli, M. Cortés, F. Crespi, G. de Angelis, F. Egea, C. Fanin, S. Fantinel, A. Gadea, E. Gamba, A. Gambalonga, C. Gesmundo, G. Gosta, A. Gottardo, A. Gozzelino, E. Gregor, M. Gulmini, J. Ha, K. Hadyńska-Klek, A. Illana, R. Isocrate, G. Jaworski, P. John, S. Lenzi, S. Leoni, S. Lunardi, M. Magalini, N. Marchini, B. Million, V. Modamio, A. Nannini, D. Napoli, G. Pasqualato, J. Pellumaj, R. Pérez-Vidal, S. Pigliapoco, M. Polettini, C. Porzio, A. Pullia, L. Ramina, G. Rampazzo, M. Rampazzo, M. Rebeschini, K. Rezynkina, M. Rocchini, M. Romanato, D. Rosso, A. Saltarelli, M. Scarcioffolo, M. Siciliano, D. Testov, D. Tomasella, F. Tomasi, N. Toniolo, C. Ur, S. Ventura, F. Veronese, E. Viscione, V. Volpe, O. Wieland, I. Zanon, S. Ziliani, G. Zhang, D. Bazzacco, The GALILEO γ-ray array at the legnaro national laboratories, Nucl. Instrum. Methods Phys. Res. Sect. A: Accel. Spectrometers, Detect. Assoc. Equip. 1015 (2021) 165753.

[47] G. Gosta, A. Mentana, F. Camera, A. Bracco, S. Ceruti, G. Benzoni, N. Blasi, S. Brambilla, S. Capra, F.C.L. Crespi, A. Giaz, S. Leoni, B. Million, S. Riboldi, C. Porzio, S. Ziliani, O. Wieland, A. Nannini, M. Rocchini, N. Marchini, M. Ciemała, M. Kmiecik, A. Maj, B. Wasilewska, M. Zieblinski, D. Filipescu, J. Kaur, N. Marginean, S. Pascu, T. Glodariu, D. Ghita, V. Zamfir, J.J. Valiente-Dobón, G. de Angelis, F. Galtarossa, A. Goasduff, T. Bayram, A. Gadea, A. Montaner, I. Zanon, D. Brugnara, A. Gozzelino, G. Pasqualato, R. Menegazzo, A. Gottardo, G. Jaworski, S. Lenzi, D. Napoli, D. Testov, M. Siciliano, T. Marchi, D. Mengoni, D. Bazzacco, A. Boso, P.R. John, F. Recchia, R. Raabe, O. Poleshchuk, J. Yang, Probing isospin mixing with the giant dipole resonance in the ^{60}Zn compound nucleus, Phys. Rev. C 103 (2021) L041302.

[48] J.N. Bahcall, Neutrino Astrophysics, Cambridge University Press, Cambridge [Eng.] ; New York, 1989.

[49] Borexino Collaboration, M. Agostini, K. Altenmüller, S. Appel, V. Atroshchenko, Z. Bagdasarian, D. Basilico, G. Bellini, J. Benziger, R. Biondi, D. Bravo, B. Caccianiga, F. Calaprice, A. Caminata, P. Cavalcante, A. Chepurnov, D. D'Angelo, S. Davini, A. Derbin, A. Di Giacinto, V. Di Marcello, X.F. Ding, A. Di Ludovico, L. Di Noto, I. Drachnev, A. Formozov, D. Franco, C. Galbiati, C. Ghiano, M. Giammarchi, A. Goretti, A.S. Göttel, M. Gromov, D. Guffanti, A. Ianni, A. Ianni, A. Jany, D. Jeschke, V. Kobychev, G. Korga, S. Kumaran, M. Laubenstein, E. Litvinovich, P. Lombardi, I. Lomskaya, L. Ludhova, G. Lukyanchenko, L. Lukyanchenko, I. Machulin, J. Martyn, E. Meroni, M. Meyer, L. Miramonti, M. Misiaszek, V. Muratova, B. Neumair, M. Nieslony, R. Nugmanov, L. Oberauer, V. Orekhov, F. Ortica, M. Pallavicini, L. Papp, L. Pelicci, Ö. Penek, L. Pietrofaccia, N. Pilipenko, A. Pocar, G. Raikov, M.T. Ranalli, G. Ranucci, A. Razeto, A. Re, M. Redchuk, A. Romani, N. Rossi, S. Schönert, D. Semenov, G. Settanta, M. Skorokhvatov, A. Singhal, O. Smirnov, A. Sotnikov, Y. Suvorov, R. Tartaglia, G. Testera, J. Thurn, E. Unzhakov, F.L. Villante, A. Vishneva, R.B. Vogelaar, F. von Feilitzsch, M. Wojcik, M. Wurm, S. Zavatarelli, K. Zuber, G. Zuzel, Experimental evidence of neutrinos produced in the CNO fusion cycle in the Sun, 587 (7835) (2020) 577–582.

[50] G. Imbriani, H. Costantini, A. Formicola, D. Bemmerer, R. Bonetti, C. Broggini, P. Corvisiero, J. Cruz, Z. Fülöp, G. Gervino, A. Guglielmetti, C. Gustavino, G. Gyürky, A.P. Jesus, M. Junker, A. Lemut, R. Menegazzo, P. Prati, V. Roca, C. Rolfs, M. Romano, C. Rossi Alvarez, F. Schümann, E. Somorjai, O. Straniero, F.

Strieder, F. Terrasi, H.P. Trautvetter, A. Vomiero, S. Zavatarelli, The bottleneck of CNO burning and the age of Globular Clusters, Astron. Astrophys. 420 (2) (2004) 625–629.

[51] B. Acharya, M. Aliotta, A. Balantekin, D. Bemmerer, C. Bertulani, A. Best, C. Brune, R. Buompane, L. Gialanella, F. Cavanna, J. Chen, J. Colgan, A. Czarnecki, B. Davids, R. deBoer, F. Delahaye, R. Depalo, A. Guglielmetti, A. García, R. Robertson, M. Gatu Johnson, D. Gazit, U. Greife, D. Guffanti, K. Hambleton, W. Haxton, Y. Herrera, A. Serenelli, M. Huang, C. Iliadis, K. Kravvaris, M. La Cognata, K. Langanke, L. Marcucci, T. Nagayama, K. Nollett, D. Odell, G. Orebi Gann, D. Piatti, M. Pinsonneault, L. Platter, G. Rupak, M. Sferrazza, T. Szücs, X. Tang, A. Tumino, F. Villante, A. Walker-Loud, X. Zhang, K. Zuber, Solar fusion III: New data and theory for hydrogen-burning stars, Rev. Modern Phys. 97 (3) (2025).

[52] M. Marta, E. Trompler, D. Bemmerer, R. Beyer, C. Broggini, A. Caciolli, M. Erhard, Z. Fülöp, E. Grosse, G. Gyürky, R. Hannaske, A.R. Junghans, R. Menegazzo, C. Nair, R. Schwengner, T. Szücs, S. Vezzú, A. Wagner, D. Yakorev, Resonance strengths in the ^{14}N(p,γ)^{15}O and ^{15}N(p,$\alpha\gamma$)^{12}C reactions, Phys. Rev. C 81 (2010) 055807.

[53] C. Tsopelas, S. Brundell, B. Chatterton, A simple and inexpensive preparation of [51Cr]-MAA particles, Nucl. Med. Biol. 28 (3) (2001) 339–344.

[54] T.W. Conlon, Nuclear physics for materials technology accelerator based methods? Contemp. Phys. 26 (6) (1985) 521–558.

[55] L. Csedreki, G. Ciani, J. Balibrea-Correa, A. Best, M. Aliotta, F. Barile, D. Bemmerer, A. Boeltzig, C. Broggini, C. Bruno, A. Caciolli, F. Cavanna, T. Chillery, P. Colombetti, P. Corvisiero, T. Davinson, R. Depalo, A. Di Leva, Z. Elekes, F. Ferraro, E. Fiore, A. Formicola, Z. Fülöp, G. Gervino, A. Guglielmetti, C. Gustavino, G. Gyürky, G. Imbriani, Z. Janas, M. Junker, I. Kochanek, M. Lugaro, P. Marigo, E. Masha, C. Mazzocchi, R. Menegazzo, V. Mossa, F. Pantaleo, V. Paticchio, R. Perrino, D. Piatti, P. Prati, L. Schiavulli, K. Stöckel, O. Straniero, T. Szücs, M. Takács, F. Terrasi, S. Zavatarelli, Characterization of the LUNA neutron detector array for the measurement of the ^{13}C(α,n)^{16}O reaction, Nucl. Instrum. Methods Phys. Res. Sect. A: Accel. Spectrometers, Detect. Assoc. Equip. 994 (2021) 165081.

[56] A. Koning, S. Hilaire, S. Goriely, TALYS: modeling of nuclear reactions., Eur. Phys. J. A 59 (2023) 131.